

METALLIZATION OF HIGH DENSITY POLYURETHANE SURFACES

A THESIS SUBMITTED TO
THE GRADUATE SCHOOL OF NATURAL AND APPLIED SCIENCES
OF
MIDDLE EAST TECHNICAL UNIVERSITY

BY

BÜŞRA AYKAÇ

IN PARTIAL FULFILLMENT OF THE REQUIREMENTS
FOR
THE DEGREE OF MASTER OF SCIENCE
IN
METALLURGICAL AND MATERIALS ENGINEERING

DECEMBER 2019

Approval of the thesis:

METALLIZATION OF HIGH DENSITY POLYURETHANE SURFACES

submitted by **BÜŞRA AYKAÇ** in partial fulfillment of the requirements for the degree of **Master of Science in Metallurgical and Materials Engineering Department, Middle East Technical University** by,

Prof. Dr. Halil Kalıpçılar
Dean, Graduate School of **Natural and Applied Sciences**

Prof. Dr. C. Hakan Gür
Head of Department, **Met. and Mat. Eng.**

Prof. Dr. İshak Karakaya
Supervisor, **Met. and Mat. Eng., METU**

Assist. Prof. Dr. Metehan Erdoğan
Co-Supervisor, **Metallurgical and Materials Engineering, AYBU**

Examining Committee Members:

Prof. Dr. Arcan Fehmi Dericioğlu
Metallurgical and Materials Engineering, METU

Prof. Dr. İshak Karakaya
Met. and Mat. Eng., METU

Prof. Dr. Cihangir Duran
Metallurgical and Materials Engineering, AYBU

Assist. Prof. Dr. Metehan Erdoğan
Metallurgical and Materials Engineering, AYBU

Assoc. Prof. Dr. Mert Efe
Metallurgical and Materials Engineering, METU

Date: 03.12.2019

I hereby declare that all information in this document has been obtained and presented in accordance with academic rules and ethical conduct. I also declare that, as required by these rules and conduct, I have fully cited and referenced all material and results that are not original to this work.

Name, Surname: Būşra Aykaç

Signature:

ABSTRACT

METALLIZATION OF HIGH DENSITY POLYURETHANE SURFACES

Aykaç, Büşra

Master of Science, Metallurgical and Materials Engineering

Supervisor: Prof. Dr. İshak Karakaya

Co-Supervisor: Assist. Prof. Dr. Metehan Erdoğan

December 2019, 72 pages

Electroplating onto polymeric materials is required for different purposes in various applications. Commercial polyurethanes (PU) are electrically insulator materials and durable at high temperatures. Nevertheless, the PU used in this study has high electrical conductivity, a low thermal expansion coefficient and is a high density foam. In this work, surface metallization of PU foam was studied to prepare the surface for a subsequent electroplating process. The surface metallization was carried out by sensitization, activation and electroless nickel plating. Metallized surfaces were characterized after electrochemical nickel plating at different current densities and surface morphology, roughness as well as physical properties of the coatings. The results show that increasing current density adversely affects the surface morphology and metallization processes enhance the surface conductivity of the foam.

Keywords: Surface Metallization, Electroless Nickel Plating, Nickel Electrodeposition

ÖZ

YÜKSEK YOĞUNLUKLU POLİÜRETAN YÜZEYLERİN METALİZASYONU

Aykaç, Büşra
Yüksek Lisans, Metalurji ve Malzeme Mühendisliği
Tez Danışmanı: Prof. Dr. İshak Karakaya
Ortak Tez Danışmanı: Dr. Öğr. Üyesi Metehan Erdoğan

Aralık 2019, 72 sayfa

Çeşitli uygulamalarda farklı amaçlar için polimerik malzemeler üzerine elektrokimyasal kaplama yapılmaktadır. Ticari poliüretanlar (PU) elektriksel iletkenliği çok düşük ve yüksek sıcaklık dayanımı yüksek bir polimerdir. Ancak, bu çalışmada kullanılan PU yüksek bir elektriksel iletkenliğe, düşük bir termal genleşme katsayısına sahip ve yüksek yoğunluklu bir köpüktür. Bu çalışmada, yüzeyi ardından yapılacak elektrokimyasal işlemlere hazır hale getirmek için PU'ın yüzey metalizasyonu yapılmıştır. Yüzey metalizasyonu hassaslaştırma, aktive etme ve akımsız nikel kaplama işlemlerini içeren bir prosestir. Metalize yüzeylerin yüzey morfolojileri, yüzey pürüzlülüğü ve fiziksel özellikleri farklı akım yoğunluklarında yapılan elektrolitik nikel kaplama sonrası karakterize edilmiştir. Elde edilen sonuçlara göre, akım yoğunluğundaki artışın yüzey morfolojisini olumsuz etkilediği görülmüştür ve hassaslaştırma ve ardından yapılan aktivasyon işlemi köpüğün yüzey iletkenliğini artırmaktadır.

Anahtar Kelimeler: Akımsız Nikel Kaplama, Elektrolitik Nikel Kaplama, Yüzey Metalizasyonu

To My Mommy

ACKNOWLEDGEMENTS

I would first like to thank my thesis advisor Prof. Dr. İshak Karakaya and co-advisor Asisst. Prof. Dr. Metehan Erdoğan. My professors had always faith in my capability. They encourage me to work hard and believe me that I will do the right things when I encounter problems.

Furthermore, I would also like to express my gratitude to my managers in Turkish Aerospace Inc. Ali İhsan Öz and Remzi Ecmel Ece, who gave the permission and financial support to use all required equipments and the necessary materials to complete my master thesis. I would also like to thank Bilkent University-UNAM for the characterization equipment. Moreover, I thank the DUNA Corradini S.P.A team; Mr. Giuliano Casselli and Massimiliano Motta for their technical support.

Many thanks goes to Bilgehan Çetinöz, Mertcan Başkan, Mustafa Anıl Yıldırım, Berkay Çağan and Bengisu Akpınar for their support and assistance throughout this thesis. I must express my very profound gratitude to Mustafa Serdal Aras and Esra Sütçü for providing me with unfailing support, continuous encouragement and never ending friendship throughout my years of study.

Special thanks goes to Dr. Yahya Öz; the most humorous physicist I know for the stimulating discussions, his help as well as support and for all the fun we had.

I must express my very profound gratitude to my brother/sister-like friends İstemihan Gökdağ, Kaan Yütük and Selim Dinçer for their support and sincere friendship.

I would like to express my very profound gratitude to the love of my life for providing me unfailing support, continuous encouragement and deep love throughout my years of study. This accomplishment would not have been possible without him. Last but not the least, I would like to thank my family for supporting me spiritually and continuous encouragement throughout my life.

TABLE OF CONTENTS

ABSTRACT	v
ÖZ	vi
ACKNOWLEDGEMENTS.....	ix
TABLE OF CONTENTS	x
LIST OF TABLES.....	xiii
LIST OF FIGURES	xiv
1. INTRODUCTION.....	1
1.1. Importance of Composite Manufacturing for the Aerospace Industry	1
1.2. Aerospace Tooling Materials	2
1.3. Importance of Nickel for Tooling	3
1.4. Surface Metallization Mechanism	5
1.5. Principles of Electroless & Electrolytic Nickel Plating	9
1.6. Aim of Study.....	14
2. MATERIALS AND METHODS	17
2.1. Materials.....	17
2.2. Electroplating of PU.....	17
2.2.1. Surface Preparation Procedure	19
2.2.1.1. Grinding	19
2.2.1.2. Cleaning, Degreasing and Etching	19
2.2.1.3. Surface Sensitization	20
2.2.1.4. Surface Activation	20
2.2.2. Electroless Nickel Plating	21

2.2.3. Electrolytic Nickel Plating.....	22
2.3. Characterization of neat PU.....	23
2.3.1. Microstructural Characterization of PU.....	23
2.3.1.1. Dilatometry Analysis of PU.....	24
2.3.1.2. Thermo - Gravimetric Analysis (TGA) of PU.....	25
2.3.1.3. Surface Morphology Analysis of PU.....	26
2.3.1.4. Surface Roughness of PU.....	27
2.3.2. Electrical Characterization of PU.....	28
2.3.2.1. Physical Property Measurement System (PPMS) Analysis of PU.....	29
2.4. Characterizations of Metallized PU Surfaces.....	33
2.4.1. Microstructural Characterization of Metallized PU Surfaces.....	35
2.4.1.1. Surface Morphology Analysis of Metallized PU Surfaces.....	35
2.4.1.2. Roughness Measurement of Metallized PU Surfaces.....	35
2.4.1.3. XPS Analysis of Metallized PU Surfaces.....	35
2.4.1.4. XRD Analysis of Metallized PU Surfaces.....	36
2.4.2. Electrical Characterization of Metallized PU Surfaces.....	37
2.4.2.1. Physical Property Measurement System (PPMS) Analysis of Metallized PU Surfaces.....	37
3. RESULTS AND DISCUSSION.....	39
3.1. Characterization of a Metallized PU Surface at Each Step.....	39
3.1.1. Microstructural Characterization.....	39
Surface morphology, surface roughness, XPS and XRD analyses of samples after each metallization step are mentioned briefly in the sections below.....	39
3.1.2. Surface Morphology Analysis.....	39

3.1.3. Surface Roughness Measurement	50
3.1.4. XPS Analysis.....	52
3.1.5. XRD Analysis.....	54
3.1.6. Electrical Characterization	56
3.1.6.1. Physical Property Measurement System (PPMS) Analysis.....	57
4. CONCLUSION	61
REFERENCES	63
A. List of Chemicals.....	71
B. MATLAB Code for PPMS Measurement	72

LIST OF TABLES

TABLES

Table 1.1. The Sulphamate Electrolyte Specification [52]	13
Table 2.1. Levels and Parameters Used in the Design of Experiment.....	23
Table 2.2. List of Surface Metallization Processes and Contractions used for Identification	33
Table 3.1 The Current Efficiencies for Each Step	44
Table 3.2. The SEM Views of Electrolytic Ni Plated Surfaces with a Current Density of 3 A/dm ²	48
Table 3.3. Scherrer Calculation for each Surface Metallization Process	56

LIST OF FIGURES

FIGURES

Figure 1.1. Micro-Hardness of Electroless Nickel Coatings Deposited Under Various Polishing Conditions of the CFRP Substrate [24]	6
Figure 1.2. Surface Roughness of Electroless Nickel Coatings Deposited Under Various Polishing Conditions of the CFRP Substrate [24]	7
Figure 1.3. The Thickness of Electroless Nickel Coatings Deposited Under Various Polishing Conditions Of The CFRP Substrate [24]	7
Figure 1.4. The Mössbauer Spectroscopy of Sn Layers of Kapton Foil a) Sn Sensitized b) Sn Sensitized and UV Exposed c) Sn Sensitized and Pd Activated. The Divalent and Tetravalent Sn Ions' Relative Amounts are Related To Areas Under Spectral Lines [41].....	8
Figure 1.5. The Homogeneity Difference of Electroless and Electrolytic Plating [48]	10
Figure 1.6. Schematic Drawing of Nickel Electroplating Cell	12
Figure 1.7. Schematic Drawing of Steps for The Nickel Lay-Up Tool Manufacturing Process	15
Figure 2.1. Processes and Characterizations Chart. Note That Each Number is Linked to Table 2.2.	18
Figure 2.2. The Change of Thermal Expansion Coefficient with respect to Temperature	25
Figure 2.3. Thermal Decomposition of Neat PU	26
Figure 2.4. The Surface Morphology and Pore Size of Neat PU	27
Figure 2.5. The Surface Roughness of Neat PU Before Grinding ($R_a=6.14 \mu\text{m}$).....	28
Figure 2.6. The Surface Roughness of Grinded PU After Grinding ($R_a= 1.91 \mu\text{m}$). 28	
Figure 2.7. a) Preferred and b) Acceptable Geometries of the Sample for a PPMS Measurement.....	29
Figure 2.8. The Sample Configuration of Van der Pauw Measurement	30
Figure 2.9. The Scanning Configuration Matrices of Van der Pauw Measurements	31

Figure 2.10. The Bulk Resistivity of Neat PU Foam	33
Figure 3.1. The SEM Images of Sensitized and Activated Samples; a) Sn Sensitized, b) PdCl ₂ and c) PdCl ₂ * Activated Samples.....	40
Figure 3.2. Surface Morphology of the PdCl ₂ * Activated Sample. Note that in this figure the magnification is 5000x. In comparison with the Sn sensitized surface Pd is observable.	40
Figure 3.3. EDS Analysis of Sn Sensitized and Pd Activated Samples.....	41
Figure 3.4. The Change in the Surface Roughness of the PU Substrate a) After Alkaline Electroless Ni Plating with 0.5 g/L PdCl ₂ and b) 1 g/L PdCl ₂ Activation Solution c) After Acidic Electroless Ni Plating with 0.5 g/L PdCl ₂ and d) 1 g/L PdCl ₂ Activation Solution	52
Figure 3.5. XPS Analysis of Each Sample. Note the Sn3d5 peak which indicates the presence of Sn ⁴⁺ for the PdCl ₂ sample and the high Sn3d peak for the Sn sample which shows that Sn ²⁺ does not oxidize completely [71].	54
Figure 3.6. XRD Analysis of Each Sample.....	55
Figure 3.7. The Change in the Crystallite Size with respect to the Surface Metallization Process	56
Figure 3.8. The PPMS Measurement of Sn Sensitized Sample in Contrast to Neat PU	58
Figure 3.9. The PPMS Measurement of Metallized Samples	59

CHAPTER 1

INTRODUCTION

1.1. Importance of Composite Manufacturing for the Aerospace Industry

Composite part manufacturing is playing a key role for the aerospace industry due to its high strength to weight ratio, high fatigue performance, high impact resistance, high damage tolerance and low corrosion problems [1-6].

Composite materials can be used both for secondary and primary parts of aircrafts. Especially, Carbon Fiber Reinforced Polymers (CFRP) and Glass Fiber Reinforced Polymers are the most preferred composites because they include relatively strong, stiff carbon and glass fibers in a tough resin matrix and enable aircraft designers and manufacturers to use them as primary parts [7]. There are several methods for composite part manufacturing, i.e; injection molding, resin transfer molding, compression molding, filament winding, fiber placement, automated type laying, pultrusion and the most commonly used method; hand lay-up with thermoset resin pre-impregnated fibers (prepreg).

For hand lay-up processes, prepregs are layed up onto the composite lay-up tools and taken to the autoclave under high temperature and pressure to cure/crosslink the thermoset matrix. Thus, composite lay-up tools play an important role for composite manufacturing. There are many composite tooling materials that are used for manufacturing different parts. For both manual and automated lay-up processes, prepregs are layed on the tools before the autoclave treatment, which is curing of the prepreg layers under high temperature and high pressure to crosslink the layers with the thermoset resin matrix. Furthermore, mechanical properties are enhanced and a unified component is obtained by this process. The autoclave process has the key role to define the composite's properties, therefore lay-up tools should be defect free to

avoid vacuum leakage, durable at high temperature and high pressure. Moreover, lay-up tools should have low thermal expansion values for geometric tolerances during autoclave treatment. Surface properties such as scratch resistance have also notable effects. As a result of these requirements there are many different composite lay-up tool materials used in aerospace applications.

1.2. Aerospace Tooling Materials

Due to the increasing demand for tooling materials with high performance and high quality standards in advanced composite parts, new tooling materials and tool manufacturing techniques appeared to satisfy the highly specialized requirements of the composite components used in aerospace industries. The most important requirement for the tooling materials is a low coefficient of thermal expansion (CTE) and high temperature durability. Aluminium, steel and composite tools are frequently used in aerospace industries [8,9].

Nevertheless, there are some drawbacks of aluminum, steel and CFRP composite tools. Especially for aluminium tools, the most important one is the distortion problem due to the thermal expansion difference between the prepreg and tool after the curing process [9,10]. To overcome the distortion problem, CFRP composite tools are used for complex shaped parts. Manufacturing of these CFRP composite tools includes several steps and unfortunately the manufacturing time increases [11]. The main procedure of the CRFP composite tool manufacturing route is as follows: Epoxy tooling boards are gathered and attached to each other and machined as negative geometry of the final tool, named as master model. Thus, CFRP prepregs lay-up with the rule of balance and symmetry to the master model and are cured for several steps. The part is separated from its master model and used as composite lay-up tool finally. The main drawback of CFRP composite tool is its lifetime. Under variable cure cycles, different temperatures and pressures the life time of the tool becomes shorter [12].

Due to increasing requirements of advanced composite parts, research in areas like invar and nickel tool manufacturing technologies have been getting very popular [13].

1.3. Importance of Nickel for Tooling

Manufacturing of complex shaped aircraft structures, especially for C and U spars and leading edge parts of aircrafts invar (FeNi36/64FeNi) and Nickel tools are used to overcome the distortion problem. The CTE of Invar, pure Ni and Al (6061) are 1.6, 13.3 and $23.6 \cdot 10^{-6} \text{ K}^{-1}$ respectively [14].

Invar has low CTE, however lay-up tools made by it are mostly limited with stock size since weldability of materials restricts the joining of large geometries. Hence usually it is not possible to produce large tool geometries with this material. Additionally, welding defects such as porosities, lack of fusion defects and cracks cause impurities on the joining areas which disturb vacuum conditions inside the autoclave process [15-18]. The porosity in welding areas especially at heat affected zones may affect the static test results adversely, since the success criteria of composite lay-up tools are static and dynamic tests. The static test is applied under full vacuum condition, vacuum gauge reading should not drop more than 2 inches Hg in 5 minutes for tools under 5 m^2 [19,20]. Moreover, the manufacturing costs of Invar tools are high for large scale applications [21].

Regarding the properties of Invar, nickel can be considered as a tool material. Nickel has a relatively low CTE, is durable at high temperature and pressure. The manufacturing is cost-effective and applicable for complex and large scale. Besides distortion of the nickel tool can be compensated by adjustment of the tool structure. Nickel tools have excellent heat conductivity, high surface hardness and are resistant to corrosion, erosion and minor abrasion [22,23]. Furthermore, Ni tools can be manufactured with very low tolerance (micron sensitivity) especially by the Nickel electrodeposition method [24-27].

The electrodeposition process takes place in an electrolyte which contains ions and two electrodes; cathode and anode. Under electric current, atoms are oxidized on the surface of the anode and reduced onto the surface of the cathode. The cathode is used as a substrate, referred to as mandrel, to form a composite lay-up tool.

For large scale and/or complex shaped composite tools, the use of metallic mandrel cathodes is not recommended because of machining problems and manufacturing costs, especially for radomes which have conical shapes, metallic mandrel manufacturing is not feasible. Polymeric mandrels can be used to manage the problem that originates from this need due to its ease of machinability and cost effectiveness [28-30].

However, for polymers the problems to overcome are, high electrical resistivity, low temperature durability and operating temperature [31]. In order to apply electrolytic nickel plating on a polymeric material, the surface of the cathode should conduct electricity.

The list of polymers mentioned in Mallory and Hadju's study are [32];

- Acrylonitrile-Butadiene-Styrene
- Polypropylene
- Polysulfone
- Polyethersulfone
- Polyetherimide
- Polyarylether
- Polycarbonate
- Polyphenylene oxide (modified)
- Polyacetal
- Urea formaldehyde
- Diallyl phthalate
- Mineral-reinforced nylon
- Phenolic

PU has some advantages compared to polymers listed above making it a suitable candidate for the following reasons. For shock applications, acoustic and thermal insulation properties of PU foams are used due to its high energy absorption property. Thus, PU foams have been used in the automobile, building, packaging and

importantly in the aircraft industry [33]. To improve the performance and increase the application area of the foam, a layer of metallic coating is applied on the surface of PU. Thus, the surface of the foam is expected to be electrically conductive. The conductive surface of the foam can be plated by the electrodeposition method. Moreover, the ultimate goal of Nickel tool manufacturing is commercial availability. Among these requirements, the electrolytic Nickel plating method is deemed suitable for the Ni lay-up tool manufacturing process. The abovementioned superior properties of PU foams as a mandrel material for the Ni lay-up tool manufacturing process makes PU foam a suitable candidate for mandrels for large and complex components. Due to low chemical activity and low electrical conductivity, the surface of the foam can be metallized and electrolytically plated.

1.4. Surface Metallization Mechanism

Surfaces of high density polyurethane foams were metallized for the purpose of production of an appropriate mandrel material in this presented work. PU used in this study has a low coefficient of thermal expansion, high durability at high temperatures and is especially designed for direct lay-up tools for composite manufacturing processes [73]. The high thermal conductivity and low thermal expansion coefficient properties are the most advantageous features of tooling materials for composite manufacturing. It reduces manufacturing time and tooling costs. The stability of the polymer at high temperatures and dimensional tolerance are important parameters for the mandrel production for the subsequent electroplating procedure. Additionally, PU foam has low chemical activity; it should be pre-treated before electrolytic Ni plating.

To apply electrolytic Ni plating on a PU surface, the surface of this high density PU should be metallized to accept Ni^{+2} ions due to its low chemical activity. This process increases the plating efficiency. The metallization process is a multistep process that is carried out by degreasing, etching, sensitization with Sn^{+2} ions and activation by reducing Pd^{+2} ions to Pd. The activated surface can be immersed into the electroless plating bath or directly plated electrolytically [34]. The method of SnCl_2 sensitization

and PdCl₂ activation was firstly invented by Bergström [35]. He catalysed the surface of the substrate for an electroless Ni plating process [36]. Bergström claimed that all kind of materials can be metallized by this method except glass because glass reduces the stannous chloride (SnCl₂). Marton and Schlesinger examined the nucleation and growth of the nickel-phosphorus coating by the SnCl₂-PdCl₂ activation process on dielectric surfaces [37]. They mentioned that the estimated catalytic sites created by Pd nuclei had an average diameter of 10 Å. For metallization processes the surface morphology, especially the surface roughness of the substrate plays an important role. Lee [24] indicated the optimized surface roughness values within the range of 0.9 to 1 µm of the polymeric substrate enabling the Sn⁺² atoms to adhere as the rough regions. The mechanical, electrochemical and wear properties of Ni coating on a CFRP composite were examined by Lee. He stated that the low micro-porosity, hardness (Figure 1.1.), smooth morphology (Figure 1.2.) and high thickness (Figure 1.3.) of electroless Ni coatings were obtained upon grinding the surface of the CFRP composite with 800 grade emery paper in the order of 80-120-220-400-800 # emery paper.

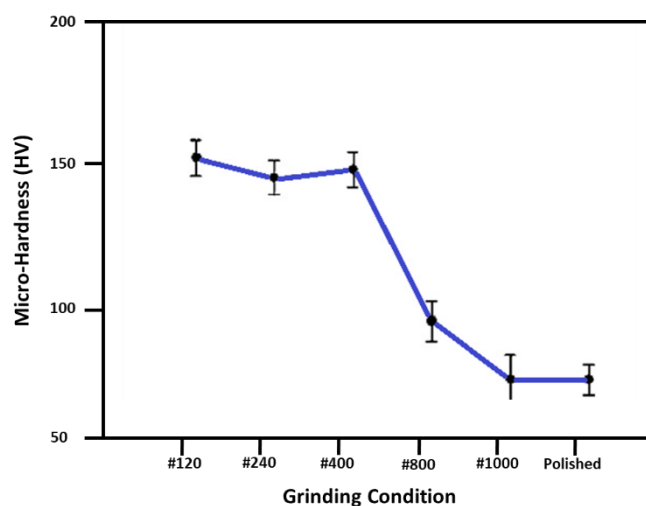


Figure 1.1. Micro-Hardness of Electroless Nickel Coatings Deposited Under Various Polishing Conditions of the CFRP Substrate [24]

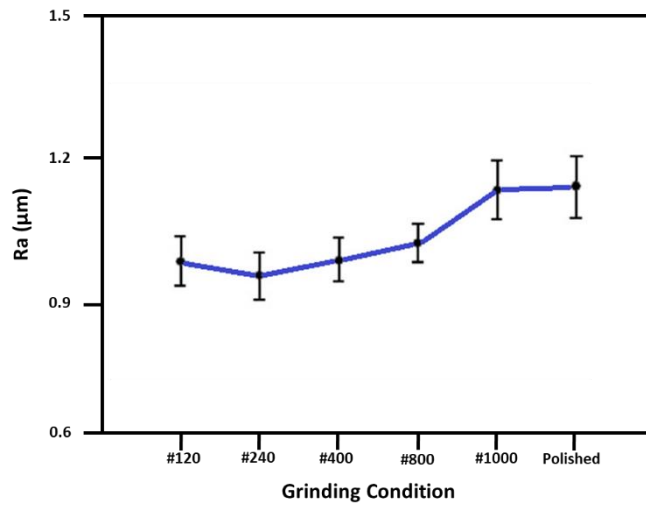


Figure 1.2. Surface Roughness of Electroless Nickel Coatings Deposited Under Various Polishing Conditions of the CFRP Substrate [24]

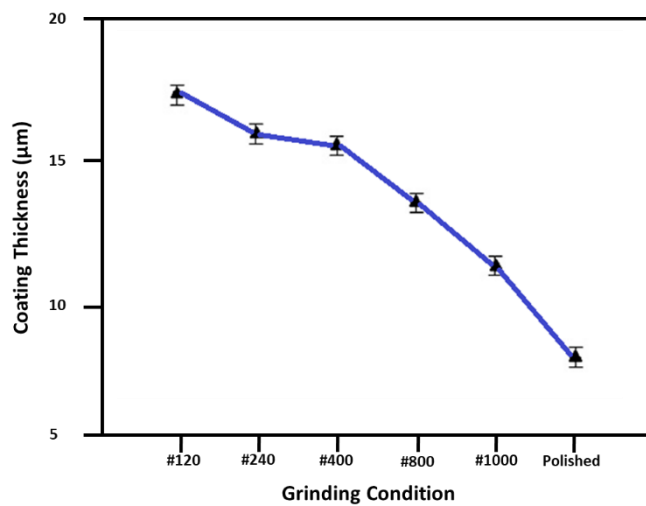


Figure 1.3. The Thickness of Electroless Nickel Coatings Deposited Under Various Polishing Conditions Of The CFRP Substrate [24]

After the grinding procedure, dirt and grease were released by rinsing in an alkaline solution. The etching is applied to increase the chemical activity and create open regions for Sn^{+2} ions for the sensitization process [32]. The other less frequently used sensitizing agents are; AgNO_3 , AuCl_3 , and metallic Na (in naphthalene solution) [42].

In the case of sensitization by tin, the Sn^{+2} ions adsorbed by porous and rough regions are present in the unstable state of Sn as Sn^{+2} [38].

In order to characterize the sensitized surface and identify the oxidation mechanism of Sn as well as its stability, Mössbauer spectroscopy was used [39]. Actually, this technique is widely used to examine the valance states of iron for mineralogy and to determine the redox ratios. The studies also show that this technique can be implemented to materials science researches [40]. Note that this technique is based on the Mössbauer effect. For this discovery, the Nobel Prize was awarded in 1961 [68].

The Mössbauer spectroscopy study of Cohen et al. [41] determined the nature of solutions during deposition on sensitized and activated Kapton surfaces. The complex colloids of an Sn sensitization solution consist primarily of Sn^{4+} cores stabilized by a Sn^{2+} outer layer. The diameter of these colloids is approximately 25-100 Å . The divalent Sn oxidizes to tetravalent Sn by oxygen exposure, ultraviolet radiation or immersion to a PdCl_2 activation solution. The Mössbauer spectra indicate that all Sn^{2+} oxidize to Sn^{4+} after immersion to an activation solution mentioned in Reaction 1. The Mössbauer spectroscopy of Kapton surfaces supports this result and shows that all of the divalent Sn ions oxidize to tetravalent Sn which can be seen as Figure 1.4.

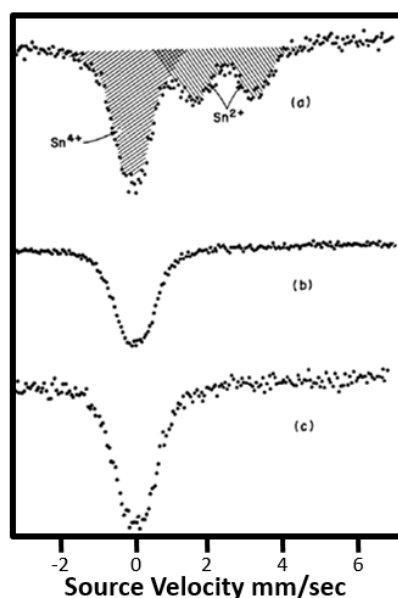


Figure 1.4. The Mössbauer Spectroscopy of Sn Layers of Kapton Foil a) Sn Sensitized b) Sn Sensitized and UV Exposed c) Sn Sensitized and Pd Activated. The Divalent and Tetravalent Sn Ions' Relative Amounts are Related To Areas Under Spectral Lines [41].



Schlesinger mentioned the activation solutions other than Pd such as; Au, Pt, Rh, Os, and Ag [42].

Additional studies show that surfaces become more active after electroless Ni plating. Meek mentioned that, during electroless Ni plating after sensitization and activation processes, chemical states or the structure of the surface changed which benefits the surface metallization [43].

During the subsequent processes, i.e. electroless and/or electrolytic Ni plating; Pd atoms act as nucleation sites for Ni^{+2} ions. Related with the density of nucleation sites, the electrolytic and/or electroless Ni plating efficiency increases [42].

1.5. Principles of Electroless & Electrolytic Nickel Plating

Electroless Ni plating is chemical reduction of Nickel ions in an aqueous solution containing a reducing agent and thus the Nickel deposits onto the substrate without usage of electrical energy.

The electroless Ni plating was invented accidentally by Brenner and Riddell, they coated nickel on the steel substrate by the efficiency of 130 % by using NaH_2PO_2 [44]. This result showed that there was some chemical reduction happening at high temperatures with hypophosphite addition. The autocatalytic (electroless) plating is defined as metallic coating deposition by reduction of metals by reducing agents. Ni, Co, Pd, Cu, Au and Ag are deposited onto the substrates without applying any current [42]. The reducing agents are; hypophosphite, Cu-hydrazine, borohydrides, amine boranes and their derivatives [45].

The mechanism of electroless Ni plating at a high temperature interval between 60 and 95 °C with sodium hypophosphite reduction is; hypophosphite reduces the metallic Ni and H_2 reduction is also observed on the surface mentioned as Reaction 2-7 described by mixed potential theory [45,46].



Electroless Ni plating lowers the porosity and roughness of the surface and thus, lowers the corrosion resistance [47] and enhances the surface quality. Thus, as mentioned in Section 1.3., the surface property of coating directly affects the static and dynamic test results of Ni tools.

Additionally, the power supply, electrical contact and the other apparatus are not required in electroless deposition. One of the most important advantage of electroless Ni plating is homogeneity of the coating as it can be seen as Figure 1.5 [48].

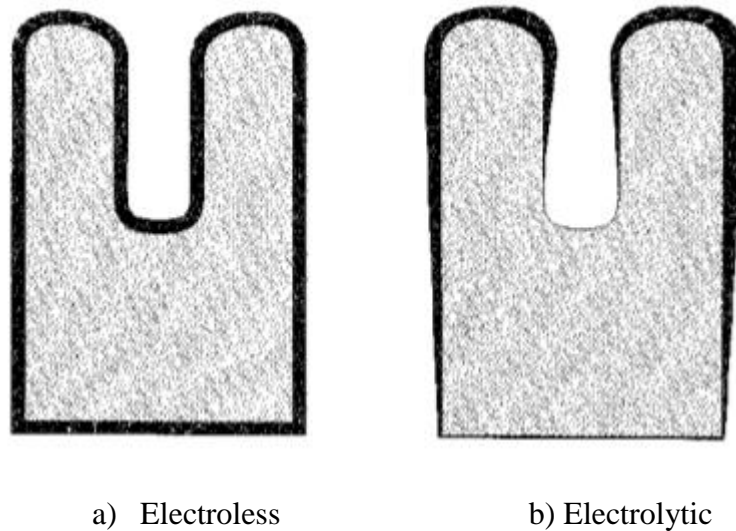


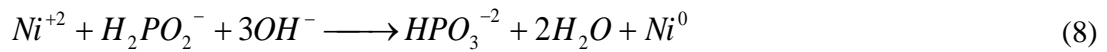
Figure 1.5. The Homogeneity Difference of Electroless and Electrolytic Plating [48]

More importantly, electroless deposition can be easily applied to the non-conductive surface because no power supply is needed. Thus, after surface metallization, Nickel atoms can be adhered directly to the nucleation sites of the Pd particles.

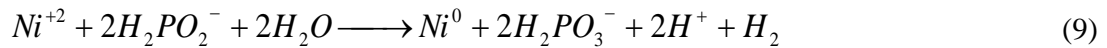
The main disadvantage of electroless Ni plating is; for mass production manufacturing time is very long when compared to the electrolytic Ni plating. Because, the stability of Nickel plating bath and Ni ions in the electrolyte decreases after a certain period of time, the sustainability of the Ni source is a problem and the coating efficiency is low in comparison to electrolytic Ni plating.

There are two different electroless plating electrolytes that are; acidic and basic. The plating reactions are mentioned as Reactions 8 and 9 [32, 45].

The overall electroless Ni plating reaction in an alkaline (basic) bath;



The acidic Ni plating overall reaction;



The schematic drawing of an electrolytic Nickel plating cell for electrodeposition is shown in Figure 1.6. The electrical current named 'I' flows through the positively charged anode to the negatively charged cathode through conductors connected to a power source and via ions in the electrolyte. The surfaces where the reduction and the oxidation take place are the cathode and anode respectively [49]. By the application of a current, reduction of Ni²⁺ ions to Ni atoms takes place on the cathode surface and deposition continues. The current flowing through the cell is directly related to the plated area, so that the current density (J) is defined as the current per unit area. Alongside of nickel reduction, hydrogen gas evolution may take place on the surface of the cathode. The hydrogen gas evolution is the secondary electrode reaction which takes place on the cathode during aqueous electroplating processes. Hydrogen evolution affects the surface morphology and structure of the coating. Hydrogen atoms may come together and form H₂ bubbles in voids or vacancies and results in the

hydrogen embrittlement problems of the coating. Thus, the hydrogen gas should be removed from the surface of the cathode by stirring mechanically or agitating continuously [50].

The uniformity of the thickness is another parameter that should be taken into account. For engineering applications homogeneity of the thickness is very important because of the manufacturing tolerances and design requirements of the parts. The distance between the cathode and anode, the positions and the shape of the anode and cathode determines the uniformity of the thickness of the coating.

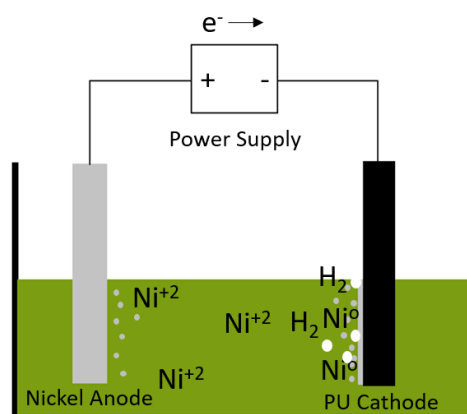


Figure 1.6. Schematic Drawing of Nickel Electroplating Cell

The electrolytic deposition of Nickel includes electrical current and as a nickel source a Ni anode. The Ni atoms are oxidized at the surface of the anode as Ni⁺² ions and carried through the electrolyte, and reduced at the surface of the cathode [25]. Meanwhile anions move to the anode surface [51].

Nickel electrodeposition is the most frequently used method for electroplating and electroforming. It is used for electronics, telecommunication, aerospace and other applications. Ni electrodeposition has superior advantages in many engineering applications i.e., high erosion and corrosion resistance, high hardness and very low internal stress. There are basically two types of electrolytes used for electrolytic deposition; Watts and Nickel Sulphamate [52].

Ni sulphamate electrolyte was used in this study because, the coatings have the lowest internal stress, high ductility and very high coating efficiency [53] compared to Watts electrolyte. The electroplating process parameters and composition can be seen in Table 1.1.

Table 1.1. *The Sulphamate Electrolyte Specification [52]*

Temperature (°C)	32-60
pH	3.5-5
Agitation	Air or mechanical
Current Density (A/dm ²)	0.5-30
Nickel Sulphamate (g/L)	300-450
Boric Acid (g/L)	30-45

The thickness measurement of electrolytic deposition is governed by Faraday's Law shown as Eq. E1. Basically, the thickness of the coating is directly proportional to the weight of the coating per unit area, W (g/dm²) [54] .

$$W = \frac{M \cdot J \cdot t}{z \cdot F} \cdot \eta \quad (\text{E1})$$

M is the molecular weight of the coating (Ni), J is current density (A/dm²), t is the time of the coating process (s), z is the valence electron, in the case of Ni taken as 2, F is Faraday's constant (96485 coulombs/mole e⁻) and η is the current efficiency of the coating process given as Eq. E2 below:

$$\eta = \frac{\text{actual weight of deposition}}{\text{theoretical weight of electrodeposition}} \quad (\text{E2})$$

The weight W , which was calculated by Eq. E1, was used for estimating the theoretical thickness T by use of Eq. E3. In this equation the specified coating area (A) is 0.05 dm² and the density (ρ) of Ni is 8.9 g/cm³.

$$T = \frac{W}{A \cdot \rho} \quad (\text{E3})$$

Cross section views taken by SEM (Scanning Electron Microscopy) were used for measuring the thickness of the coating. This experimental result was used for the determination of the weight by Eq. E3. Another approach was used by measuring the weight differences before and after the coating directly. Comparison of these two results by use of Eq. E2 yields an efficiency of 97 %. This result shows that the experimental error of the thickness measuring through SEM is quite small. Hence this method was used in this study.

1.6. Aim of Study

The main purpose of this study was to enable the way of manufacturing Ni composite lay-up tools via an electroforming method onto a PU surface. It is very important to create know-how and to define the mechanism of this process, which is significant for the aerospace industry to bring it into mass production on a large scale because understanding the background information facilitates intervention at the right time during ongoing production. The originality of this study is the application of a metallization process to prepare PU as mandrel for the electrolytic production of a Ni lay-up tool. The schematic drawing of the production of a Nickel lay-up tool via a surface metallization process is given as Figure 1.7.

This thesis is structured to understand the metallization mechanism of PU surface. For this reason, surface metallization and its effects on microstructure and electrical properties of the electroless and electrolytic Ni plating process have been characterized in detail. The thermal analysis and the electrical behaviour of PU at different stages of metallization were determined to define its behaviour at high temperatures and prepare it as substrate for preparing Ni composite lay-up tools via electroforming.

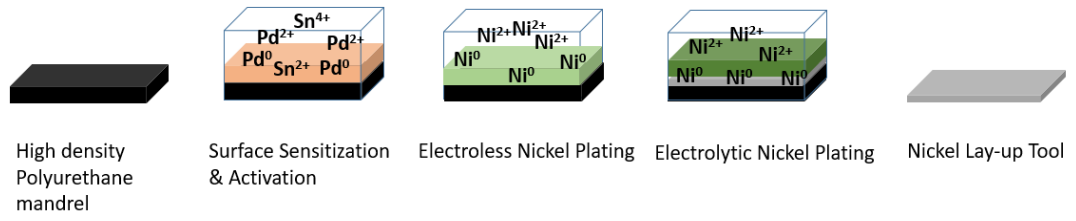


Figure 1.7. Schematic Drawing of Steps for The Nickel Lay-Up Tool Manufacturing Process

CHAPTER 2

MATERIALS AND METHODS

2.1. Materials

The materials that are used in this study together with their producers are listed in Appendix A. The substrate material and its characterization test results are given in this section.

2.2. Electroplating of PU

Surface metallization, electroless and electrolytic Ni plating methods used in this study are explained briefly in this subsection. These processes and characterization methods used along the procedure are given as Figure 2.1. The first route of the surface metallization process was to understand the effect of the Sn sensitization on electrolytic Ni plating. Hence, the surface of PU was sensitized with Sn and electrolytic Ni plating was applied directly. After sensitization the entire area of the substrate was plated for 7 hours with 2 A/dm² current density. The aimed thickness for electrolytic Ni plating for this study was 172.2 μm. This theoretical value was calculated by use of Faraday's Law (Eq. E1). Nevertheless, the actual reached thickness was below this value because of the effects of Sn sensitization. After the sensitization process, the current efficiency was measured to determine the effect of sensitization on the electrolytic Ni plating process by itself. The preliminary results show that the surface activation process was necessary for this study. The 2nd and 3rd route was to activate the surface with two different amounts of Pd²⁺ ions into the activation solution. The 4th and 6th processes were conducted by electroless Ni plating in an alkaline electrolyte after activation with 2 different Pd amounts into the solution. Additionally, 5th and 7th routes were tried out with the acidic electroless Ni plating with 2 different Pd amounts. Finally, electrolytic Ni plating was applied for all cases.

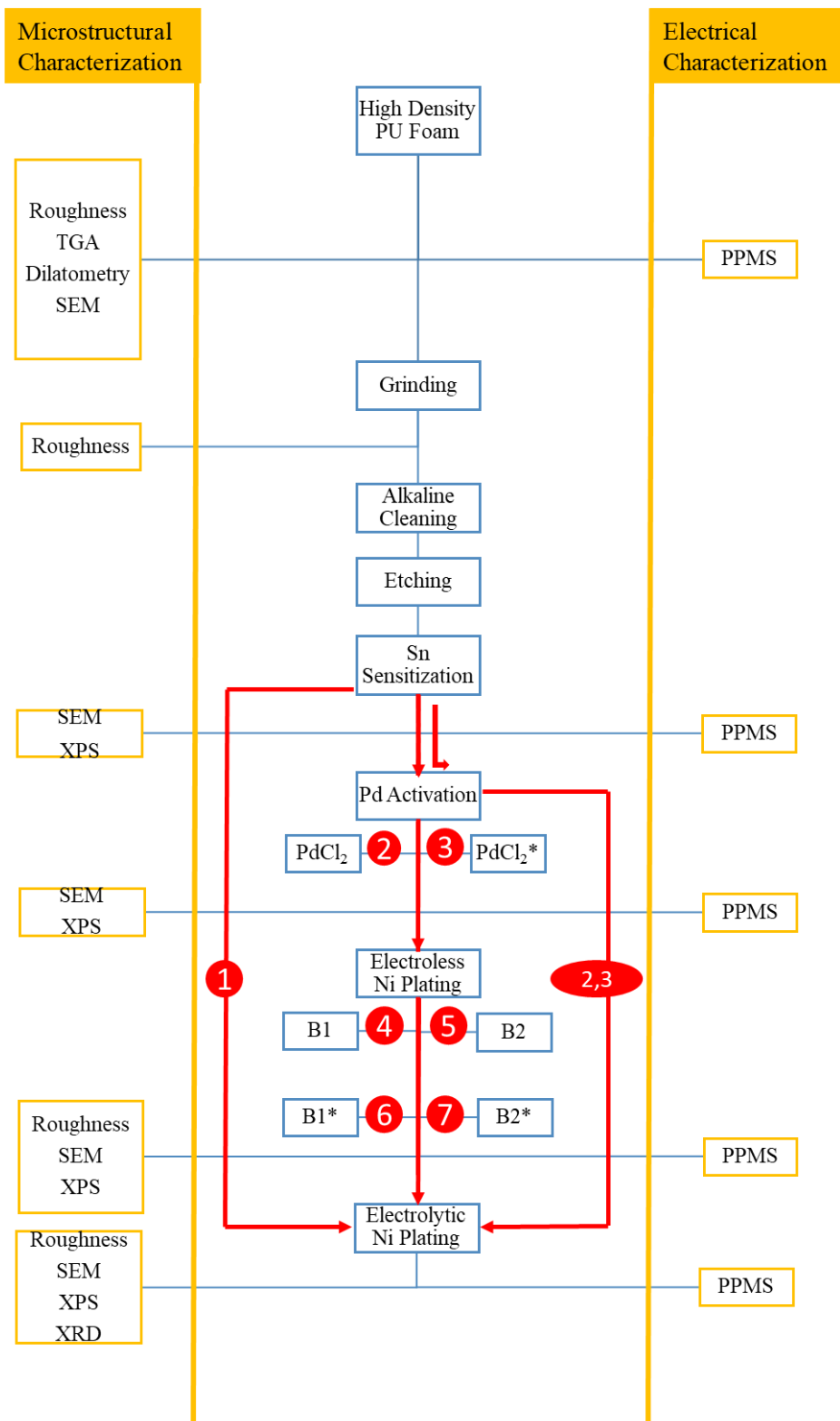


Figure 2.1. Processes and Characterizations Chart. Note That Each Number is Linked to Table 2.2.

2.2.1. Surface Preparation Procedure

Surface preparation processes of polymeric substrates are playing a crucial role for metallization processes. Therefore, the important prerequisite of the electrolytic and/or electroless Ni plating is an appropriate catalytic surface as mentioned in Section 1.4. in detail.

The surface metallization was carried out by multi-step processes which included degreasing, etching, sensitization, activation and electroless nickel plating. The effect of each step on the electroplating process and physical as well as morphological properties of the coatings were measured. Metallized surfaces were tested after the electrochemical nickel plating at different current densities. In connection with this; surface morphology, roughness as well as physical properties of the coatings were characterized. The behaviour of surface activation and sensitization steps on the mechanism of the metallization process were examined.

Since, the substrate material is porous and non-metallic, the surface was cleaned and degreased firstly, because the adsorption of particles onto the cathode surface is demanding a clean surface for subsequent steps. Thus, the effect of surface sensitization and activation on the electroless and electrolytic nickel plating process were analysed profoundly.

2.2.1.1. Grinding

The procedure started with the grinding procedure proposed by Lee et. al. [24]. The optimized grinding procedure in the order of 80-120-220-400-800 grade emery paper was followed in this study.

2.2.1.2. Cleaning, Degreasing and Etching

The surface of high density PU foam was cleaned and degreased similar to the study of Tian et. al. with alkaline solution (35 g/L NaOH, 25 g/L Na₂CO₃, 10 g/L Na₃PO₄) at 70 °C. Samples were immersed for 5 minutes to remove dirt and release grease from the surface of the mandrel firstly. After rinsing, the mandrel was submerged into the

etching solution at 45 °C for 5 minutes to prepare the surface of the foam for the sensitization procedure. The etchant was a mixture of 1 g/L KMnO₄ and 0.5 mL/L H₂SO₄ solution [55].

2.2.1.3. Surface Sensitization

The mechanism of the surface metallization process mentioned in Section 1.4. in detail states that; the Sn⁺² ions in the solution (50 g/L SnCl₂ and 1 mol/L HCl at 30 °C for 5 min) adhere into the rough and porous regions of the cathode and oxidize when the mandrel is submerged into the Pd⁺² solution and Pd is reduced on the regions where Sn⁺² ions are present. The effect of Sn sensitization before electrolytic Ni plating was examined.

After immersion in the Sn sensitization bath, the electrical resistivity was measured by use of the Van der Pauw method and the surface morphology of the sample was investigated by SEM. In addition, XPS (X-Ray Photoelectron Spectroscopy) analysis was applied and the surface chemistry was examined with nanometer sensitivity. After these microstructural and electrical characterization tests the electrolytic Ni deposition was applied and a thickness of 172.2 μm was reached theoretically. This procedure was carried out on sensitized samples with 4 different current density values. Additionally, XRD, SEM and surface roughness measurements were conducted in detail. The major points of the characterizations are simplified and given in Figure 2.1.

2.2.1.4. Surface Activation

The subsequent procedure after the sensitization process was the activation. The surface metallization was finished at this step. The Pd⁺² ions in the 2 activation solutions with different concentrations of PdCl₂ (0.5 g/L as well as 1 g/L PdCl₂ and 1 mol/L HCl at 40 °C for 5 min) were reduced by the oxidation of Sn⁺² ions. Related with the adhesivity of Sn ions, Pd ions were reduced as mentioned in Reaction 1, and the distribution of the Ni atoms were examined after electroless and/or electrolytic plating.

After immersion into Sn sensitization and Pd activation electrolytes, the electrical resistivities were measured by the Van der Pauw method and the surface morphology of the samples were investigated by SEM. In addition, XPS analysis was applied and the surface chemistry was examined with nanometer sensitivity for the purpose of understanding the behaviour of Sn after the Pd activation step.

After these microstructural and electrical characterization tests, electroless Ni depositions were applied and a thickness of 25 μm was obtained theoretically. This method was used on sensitized samples with 2 different electroless Ni plating baths. Electrolytic Ni depositions were applied at 4 different current densities. 172.2 μm thickness values were achieved theoretically. XRD, SEM, XPS, PPMS and surface roughness measurements were performed in detail.

2.2.2. Electroless Nickel Plating

The important advantage of electroless Ni plating is homogeneity of the coating mentioned in detail in Section 1.5. Moreover, after the activation process, electroless Ni plating paved the way for facilitation of electrolytic Ni plating because it enables Ni^{+2} ions to adhere easily. Two different electroless Nickel solutions were examined for the optimum results of the coating on polymeric surface. The performances of the acidic and basic solutions of electroless Ni plating processes were tested in detail. As mentioned in Section 1.5., the Pd ions acted as nucleation regions for Ni^{+2} ions to reduce in electroless plating baths. The acidic solution was Ni sulphate 45 g/L, Na hypophosphite 10 g/L, glycine 40 g/L and acetic acid 10 g/L. The pH of the solution was 4.5-5.5 and it was used at 88-95 °C for 30 minutes. Note that 25 μm coating thicknesses were aimed in accord with Nunes et al. [52]. The basic solution was, $\text{NiCl}_2 \cdot 6\text{H}_2\text{O}$ 30 g/L, Na hypophosphite 40 g/L, Na citrate 25 g/L and NH_4Cl 50 g/L. To arrange the pH in the range of 9-10 ammonia was added to the solution. The process was conducted at 86 °C for 30 minutes. Additionally, the overall reactions at the acidic and basic electrolytes are given as Eq. 2-6 in Section 1.5. The reducing agent, sodium hypophosphite was used in both acidic and basic electroless Ni plating. Electroless Ni plating both in acidic and alkaline electrolytes was applied after surface metallization

processes, before the electrolytic Ni coating at 4 different current densities in this study. The effect of surface activation composition on both alkaline and acidic electroless Ni plating bath was examined.

2.2.3. Electrolytic Nickel Plating

Electrolytic plating was applied after each step of preparation methods to determine the mechanism of surface preparation steps individually. The nickel sulphamate bath was used as electrolyte because the sulphamate electrolyte provides coatings having the lowest internal stress, highest ductility, highest deposition rate and highest purity of all nickel bath types [53]. The optimum process parameters and compositions are given in Table 1.1. In this study, Nickel electroplating was applied at 50 °C and 2 to 5 A/dm² current density. Air agitation and mechanical stirring were applied during the operation.

The experimental route formed by full factorial design using the Minitab statistical software is given as Table 2.1. In addition to this experimental design, non-metallized substrates were coated directly by electrolytic plating using 2, 3, 4 and 5 A/dm² current densities after the surfaces were sensitized with Sn²⁺ ions only. The same range of current density examined in the full factorial design of experiment built was used to lay the base for comparison.

Table 2.1. *Levels and Parameters Used in the Design of Experiment*

Factors	Electroless Ni Plating Electrolyte	PdCl₂ Amount (g/L)	Current Density (A/dm²) (J)
Level 1	N/A	0.5	2
Level 2	Alkaline Electrolyte (B1)	1*	3
Level 3	Acidic Electrolyte (B2)		4
Level 4			5

* The contractions are given in Table 2.2.

2.3. Characterization of neat PU

To determine the properties of the used mandrel material during the multi-step surface metallization and electroless and/or electrolytic Ni plating processes, PU was characterized. The thermal behavior, surface morphology and surface topology analyses were applied to the PU mandrel.

2.3.1. Microstructural Characterization of PU

The analysis of the thermal expansion coefficient was done by dilatometry, and the thermo-gravimetric analysis was done for determination of the thermal degradation of PU at temperatures up to 900 °C. Additionally, in order to measure the pore size of the PU foam, Brunauer-Emmett-Teller (BET) physisorption and chemisorption analyses were applied. However, the pore size of the foam was larger than the range of the BET analyzer in which the results are reliable. Therefore, unfortunately the results of this analysis are not reasonable. Thus, in order to measure the pore size of PU, SEM was

used. Electrical properties of neat polyurethane were examined to compare the subsequent metallization steps.

2.3.1.1. Dilatometry Analysis of PU

The determination of the coefficient of thermal expansion was done by a Dilatometry: NETZSCH DIL 402EP device. This analysis was applied to determine the linear coefficient of expansion (CTE) of PU for the range of 25-240 °C. CTE analysis was applied to 45.44 mm long BLACK CORINTHO 1100 PU foam using 5 °C/min ramping rate. The measurements are shown in Figure 2.2.

Since the surface metallization is a multistep process that is carried out by sensitization, activation, electroless and electrolytic Ni plating at variable temperatures, thermal behavior and expansion of the substrate was examined. The reason for measuring the thermal expansion of the substrate was that the substrate material for plating process is polymer. Therefore, the expansion behavior of the mandrel is important for the final product i.e. Nickel composite lay-up tool.

The thermal behavior of PU within the range of 40-90 °C yields a CTE lower than $15 \cdot 10^{-6} K^{-1}$. Commercial polyurethanes have CTE of $57.6 \cdot 10^{-6} K^{-1}$. Thus, there is smaller dimensional change in this range when above mentioned PU is used instead of commercial polyurethanes. The thermal behavior and related dimensional change reached its lowest value at approximately 85 °C. Among surface metallization and electroless and/or electrolytic Ni plating procedures, the highest process temperature was 90 °C. Therefore, a CTE value of around $5 \cdot 10^{-6} K^{-1}$ can be seen at these operating temperatures in Figure 2.2. The CTE measurement results of the present PU is quite different than commercial PU because, the relation between CTE and the temperature is; while increasing the temperature, the linear CTE of the sample tends to rise for the commercial PU case.

In the presented case, the thermal expansion and dimensional change reaches its minimum at around 85 °C. Therefore, the coating parameters did not affect the dimensions of the coating.

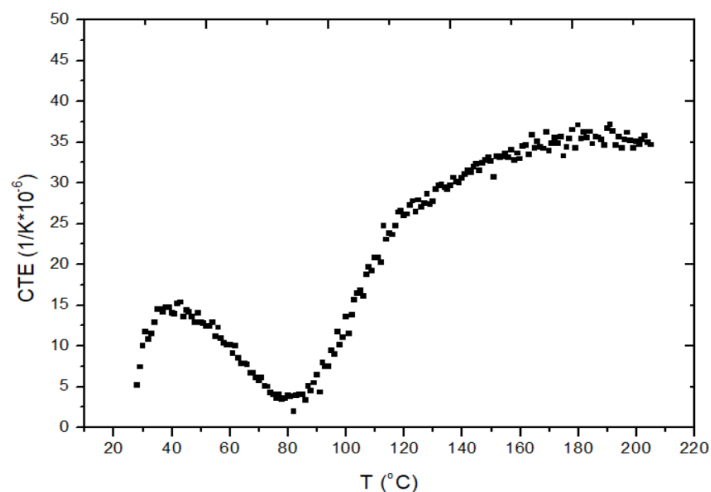


Figure 2.2. The Change of Thermal Expansion Coefficient with respect to Temperature

2.3.1.2. Thermo - Gravimetric Analysis (TGA) of PU

Thermo-gravimetric analysis involves the measurement of the change of mass of the material when temperature changes. In this study, thermal decomposition of neat PU was investigated. Therefore, thermal stability of PU foam was determined to examine the capability of surface for the metallization process. Because, a mandrel that will be produced from PU, should remain stable when it is immersed into different chemicals at different temperatures. There should not be a significant degradation at the highest temperature of surface preparation and electroless as well as electrolytic Ni coating conditions.

In order to define the thermal properties of PU, Thermo Gravimetric Analysis (TGA) was performed by: TGA Q500 V20.13 Build 39. Nitrogen gas was used (40-60 mL/min) within the temperature range of 25-900 °C at 10 °C/min heating rate. The results are given in Figure 2.3. Thus, the results showed that there was very small decomposition up to about 200 °C which can be underestimated as can be seen in Figure 2.3.

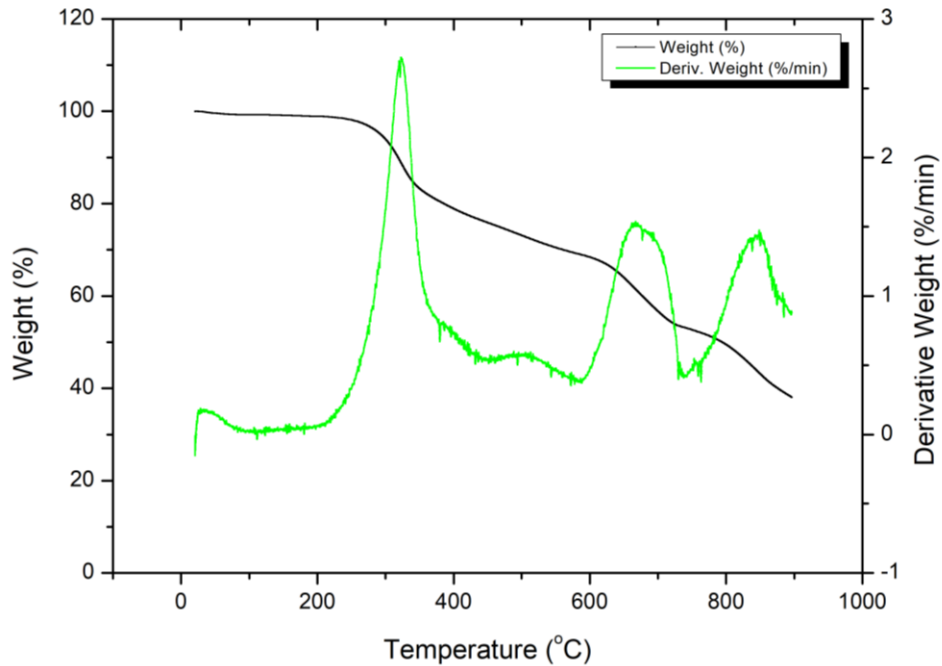


Figure 2.3. Thermal Decomposition of Neat PU

2.3.1.3. Surface Morphology Analysis of PU

Pore size of the PU foam should be determined because, the surface quality of the subsequent electroless and electrolytic plating on the PU mandrel is directly related to the surface quality of PU. The surface quality of Ni is important because, the final aim of this study was to use this Ni as composite lay-up tool for aerospace industry. Thus, the requirements mentioned in Section 1.3. should be provided. Additionally, the surface quality of coatings formed by subsequent processes was observed in detail and will be mentioned in Section 3.2.2.

Since the pore size of the foam was not detected with BET analysis as mentioned in Section 2.3.1, the variable size of pores was measured via scanning electron microscopy. The surface morphology and pore size of neat PU was analyzed by a Scanning Electron Microscope (SEM) (FEI Nova NanoSEM 430). The image that is used for measurements can be seen in Figure 2.4. The average pore size was measured as 11.32 μm .

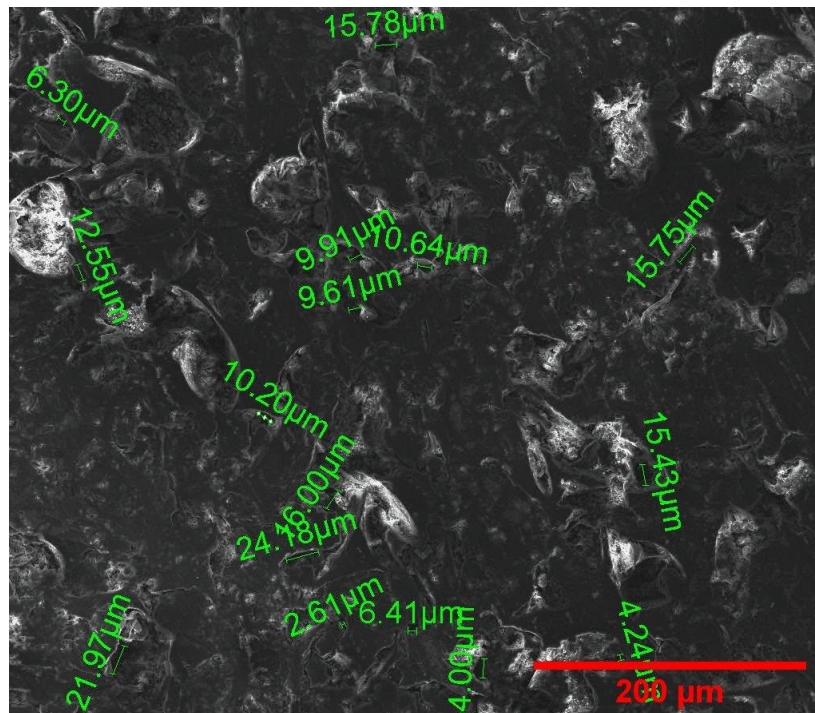


Figure 2.4. The Surface Morphology and Pore Size of Neat PU

2.3.1.4. Surface Roughness of PU

Surface topology of PU after the grinding process was measured before the metallization process. The Mitutoyo SJ400 Surface Roughness Tester (800 μm range, 8 mm evaluation length, 0.1 mm/s measuring speed) device was used to evaluate surface roughness.

Surface roughness of PU foam was measured to examine the change after grinding operation and electroless as well as electrolytic Ni plating. The surface roughness measurements were applied to 3 regions (right, middle and left) of the coupons. The initial surface roughness of neat PU was very high ($R_a = 6.14 \mu\text{m}$) as shown in Figure 2.5. However, after the grinding operation the roughness was decreased to approximately one third of the initial values as seen in Figure 2.6.

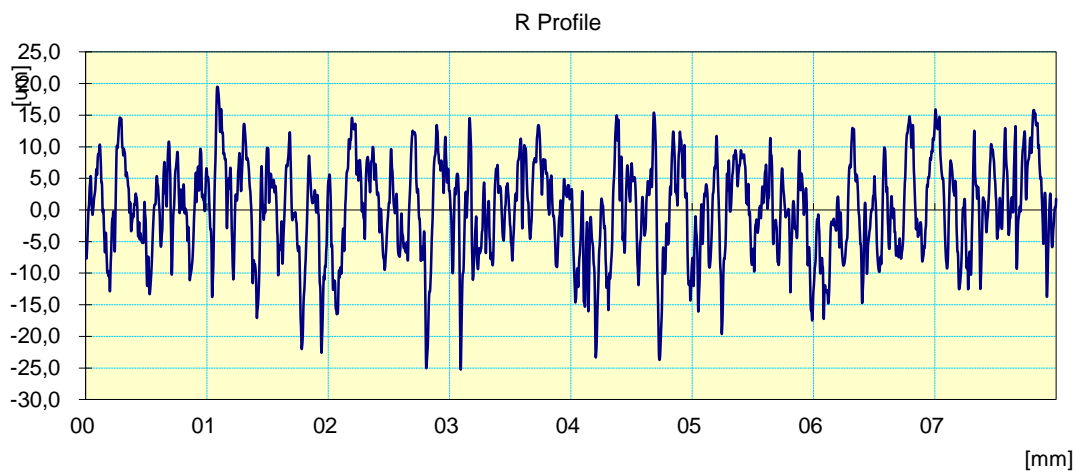


Figure 2.5. The Surface Roughness of Neat PU Before Grinding ($R_a=6.14 \mu\text{m}$)

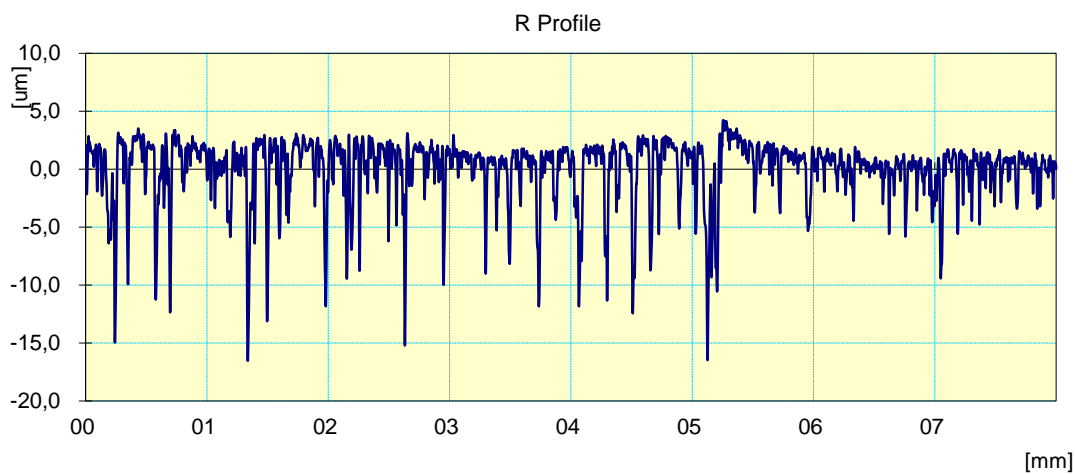


Figure 2.6. The Surface Roughness of Grinded PU After Grinding ($R_a= 1.91 \mu\text{m}$)

2.3.2. Electrical Characterization of PU

Electrical resistivity of neat PU was measured for the purpose of following the change of the electrical behavior of the mandrel during the metallization process.

2.3.2.1. Physical Property Measurement System (PPMS) Analysis of PU

There are several models for measuring the electrical resistivity of materials. The suitability of various methods and its attainable precision attach to the contact resistance and shape of the material. Among several measurement methods, the most commonly used method is four-point measurements but, the precision of this method is not so reliable compared to the Van der Pauw technique. Additionally, a four-point measurement system is used typically for low resistive and single crystal materials. Furthermore, change of the electrical resistivity with temperatures cannot be noticed properly by this method. On the other hand, Montgomery, Van der Pauw and Smith techniques are used for the pellets and bulky samples [56]. The preferred and acceptable geometries for these methods are shown in Figure 2.7.

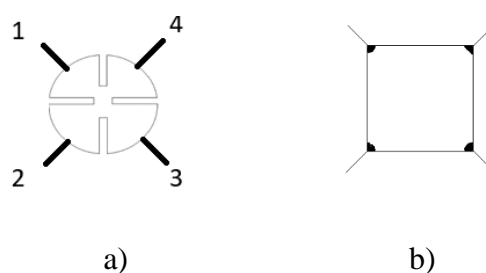


Figure 2.7. a) Preferred and b) Acceptable Geometries of the Sample for a PPMS Measurement

For PPMS measurements an acceptable geometry having $5 \cdot 5 \cdot 0.5$ mm dimensions was chosen. A cryogenic Cryogen Free Magnet System having a 9-18 Tesla high field superconducting magnet with an integrated variable temperature sample space, cryocooler(s) and compressor(s), a multi-channel temperature monitor, a sample temperature controller (Lakeshore 340) and a power supply was used.

In this study, a bulk resistivity measurement was done in the range of 298-320 Kelvin at 1 °C/min ramping rate, 0.001 A current source, magnetic field 0 Tesla and 10 V compliance voltage. Due to the geometry of the samples, there are principally 4 labelled points which can be used as contact points for measurements and can be seen in Fig. 2.8. Two of them are used for the application of a current. I_{13} is depicted along V_{24} which is the result of the measurement by use of the 2 other points. I_{13} indicates

the current passing from 3 to 1, and the voltage measured from the other 2 points is indicated by the abbreviation V_{24} . In addition, the measured resistance value for this case is shown as $R_{13,24}$. Obviously there are 16 configuration matrices. Nevertheless, there are configurations where the measured parameters just differ in sign. Hence, only 8 configurations remain. Van der Pauw measurements were applied on samples at each metallization step using 8 different scanning configuration matrices as shown in Figure 2.9

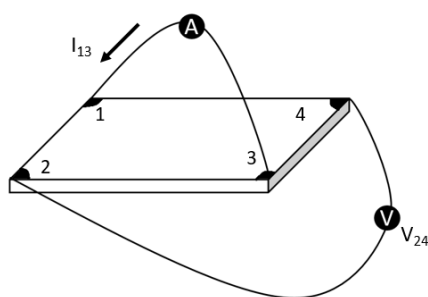


Figure 2.8. The Sample Configuration of Van der Pauw Measurement

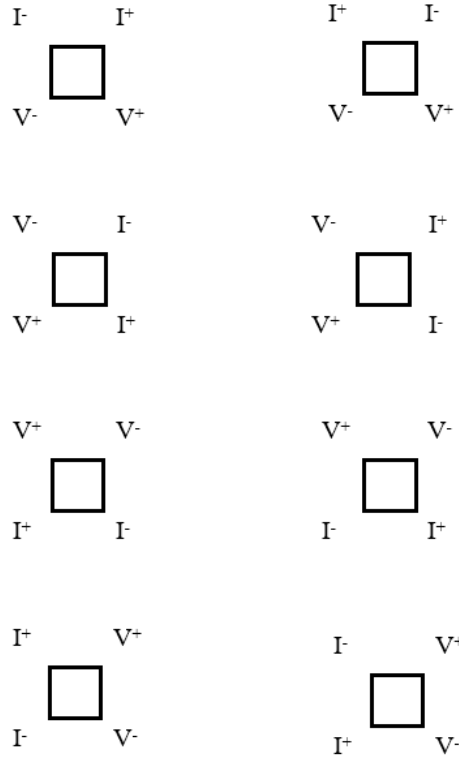


Figure 2.9. The Scanning Configuration Matrices of Van der Pauw Measurements

The basics of resistivity measurements were;

- ✓ Application of the current I_{21} and measurement of voltage V_{34}
- ✓ Reversion of the polarity of the current (I_{12}) and measurement of V_{43}
- ✓ Repeating the remaining six values (V_{41} , V_{14} , V_{12} , V_{21} , V_{23} , V_{32})

Eight measurements of voltage yield the following eight values of resistance, all of which must be positive (Eq. E4-E7):

$$R_{21,34} = V_{34} / I_{21}, \quad R_{12,43} = V_{43} / I_{12} \quad (\text{E4})$$

$$R_{32,41} = V_{41} / I_{32}, \quad R_{23,14} = V_{14} / I_{23} \quad (\text{E5})$$

$$R_{43,12} = V_{12} / I_{43}, \quad R_{34,21} = V_{21} / I_{34} \quad (\text{E6})$$

$$R_{14,23} = V_{23} / I_{14}, \quad R_{41,32} = V_{32} / I_{41} \quad (\text{E7})$$

Measurement consistency caused by current reversal requires Eq. E8 that:

$$R_{21,34} + R_{12,43} = R_{43,12} + R_{34,21} \text{ and } R_{32,41} + R_{23,14} = R_{14,23} + R_{41,32} \quad (\text{E8})$$

If any of the above fail to be true within 5 % the error source should be investigated. In this study measurements did not encounter errors as large as 5 %. The PPMS unit used in this study did not provide the resistivities of the samples directly, the resistivity values were calculated by hand and use of numerics.

Characteristic resistances (Eq. E9 and E10) R_A and R_B of each sample were calculated to determine the sheet resistivity (R_s);

$$R_A = (R_{21,34} + R_{12,43} + R_{43,12} + R_{34,21}) / 4 \quad (\text{E9})$$

$$R_B = (R_{32,41} + R_{23,14} + R_{14,23} + R_{41,32}) / 4 \quad (\text{E10})$$

The sheet resistance was calculated after the determination of the characteristic resistances by solving the Van der Pauw equation (Eq. E11) with numerical methods.

$$\exp(-\pi R_A / R_s) + \exp(-\pi R_B / R_s) = 1 \quad (\text{E11})$$

The bulk resistivity of the neat PU foam was measured from 298 to 320 K. The bulk resistivity of commercial PU shows dielectric property. However, the high density foam used in this study yields a resistivity within the range of semiconductors' as it can be seen in Figure 2.10. The resistivity of PU with increasing temperature was measured. There was no significant change with increasing temperature, the bulk specific resistance was approximately $2.2 \Omega \cdot m$. Additionally, the 320 K was the measuring limit of the PPMS. Ideally, the device would allow a measurement up to the highest temperature of the surface metallization processes. Unfortunately, the measurement range of the device does not cover all the temperatures that were used in this study. Hence, observing the behavior of PU with increasing temperature up to 320 K gives at least the temperature behavior for a certain range.

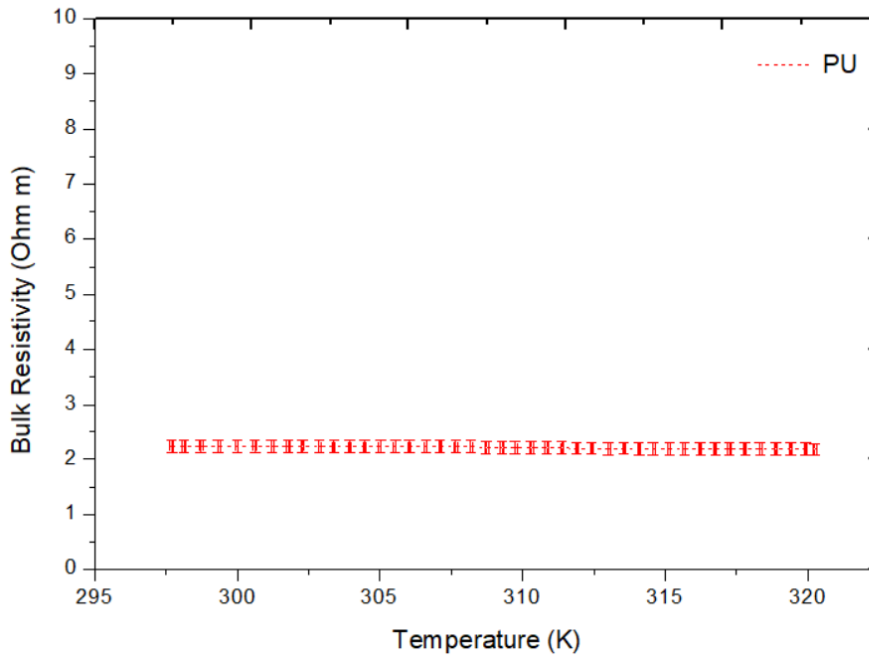


Figure 2.10. The Bulk Resistivity of Neat PU Foam

2.4. Characterizations of Metallized PU Surfaces

Microstructural and electrical characterizations of samples at each surface metallization step explained in the following sections are based on this contraction given as Table 2.2.

Table 2.2. List of Surface Metallization Processes and Contractions used for Identification

No	Surface Metallization Process	Chemical Composition	Temp. (°C)	Contraction
1	Sn Sensitization	50 g/L SnCl ₂ , 1 mol/L HCl	30	Sn
	Electrolytic Ni Plating	Nickel Sulphamate	50	
2	Sn Sensitization	50 g/L SnCl ₂ , 1 mol/L HCl	30	PdCl ₂
	PdCl ₂ Activation	0.5 g/L PdCl ₂ , 1 mol/L HCl	45	
	Electrolytic Ni Plating	Nickel Sulphamate	50	

3	Sn Sensitization	50 g/L SnCl ₂ , 1 mol/L HCl	30	PdCl ₂ *
	PdCl ₂ * Activation	1 g/L PdCl ₂ , 1 mol/L HCl	45	
	Electrolytic Ni Plating	Nickel Sulphamate	50	
4	Sn Sensitization	50 g/L SnCl ₂ , 1 mol/L HCl	30	B1
	PdCl ₂ Activation	0.5 g/L PdCl ₂ , 1 mol/L HCl	45	
	Electroless Ni Plating (Alkaline)	30 g/L NiCl ₂ *6H ₂ O, 40 g/L NaPH ₂ O ₂ , 25 g/L Na ₃ C ₆ H ₅ O ₇ , 50 g/L NH ₄ Cl	90	
	Electrolytic Ni Plating	Nickel Sulphamate	50	
5	Sn Sensitization	50 g/L SnCl ₂ , 1 mol/L HCl	30	B1*
	PdCl ₂ * Activation	1 g/L PdCl ₂ , 1 mol/L HCl	45	
	Electroless Ni Plating (Alkaline)	30 g/L NiCl ₂ *6H ₂ O, 40 g/L NaPH ₂ O ₂ , 25 g/L Na ₃ C ₆ H ₅ O ₇ , 50 g NH ₄ Cl /L	90	
	Electrolytic Ni Plating	Nickel Sulphamate	50	
6	Sn Sensitization	50 g/L SnCl ₂ , 1 mol/L HCl	30	B2
	PdCl ₂ Activation	0.5 g/L PdCl ₂ , 1 mol/L HCl	45	
	Electroless Ni Plating (Acidic)	45 g/L NiSO ₄ .6H ₂ O, 10 g/L NaPH ₂ O ₂ , 40 g/L NH ₂ CH ₂ COOH, 10 g/L CH ₃ OOH	90	
	Electrolytic Ni Plating	Nickel Sulphamate	50	

	Sn Sensitization	50 g/L SnCl ₂ , 1 mol/L HCl	30	
	PdCl ₂ * Activation	1 g/L PdCl ₂ , 1 mol/L HCl	45	
7	Electroless Ni Plating (Acidic)	45 g/L NiSO ₄ .6H ₂ O, 10 g/L NaPH ₂ O ₂ , 40 g/L NH ₂ CH ₂ COOH, 10 g/L CH ₃ OOH	90	B2*
	Electrolytic Ni Plating	Nickel Sulphamate	50	

2.4.1. Microstructural Characterization of Metallized PU Surfaces

The microstructural characterization of PU during the metallization process and after the electroless as well as electrolytic coating was done for each sample.

2.4.1.1. Surface Morphology Analysis of Metallized PU Surfaces

The surface morphology of the coating after; Sn sensitization, PdCl₂ activation, electroless Ni plating and electrolytic Ni plating performances and their cross sections are observed by using SEM adopting the parameters mentioned in Section 2.3.1.3.

2.4.1.2. Roughness Measurement of Metallized PU Surfaces

At each step of the surface preparation; the change of surface roughness was observed following the directions of ASME B46.1-2002 [72]. Before and after the electroless and electrolytic Ni plating procedures the metallization processes were examined by the method mentioned in Section 2.3.1.4. Surface roughness values were measured to determine the coating quality and coating homogeneity.

2.4.1.3. XPS Analysis of Metallized PU Surfaces

X-ray photoelectron spectroscopy (XPS) was performed by using a PHI 5000 VersaProbe. X-ray photoelectron spectroscopy technique for analyzing the surface chemistry of a material. XPS can measure the elemental composition, empirical formula, chemical state and electronic state of the elements within a material. XPS analysis was applied on samples subjected to the metallization process according to

Fig. 2.1. The surface chemistry of each sample was observed for the purpose of understanding the mechanism behind. After the surface sensitization process XPS analysis was applied for the first time. During the surface metallization steps the behavior of Sn^{+2} ions and Pd atoms as well as their states were evaluated. Pd activation was done with 2 different amounts of PdCl_2 . For the comparison of the two different kinds of processes, the surface chemistry was observed by XPS. The same procedure was utilized after the electroless Ni plated samples. The plating process was implemented with acidic and alkaline electrolytes. In conjunction with the previous surface activation processes, there were in total 4 samples to evaluate. Nevertheless, just the samples B1 and B2 were analyzed since the obtained results are also representative for the other two cases. After all, the purpose of the XPS measurement was to identify the elemental composition of the surface.

2.4.1.4. XRD Analysis of Metallized PU Surfaces

In X-Ray Diffraction analysis (XRD), a Rigaku DMAX 2200 X-ray Diffractometer equipped with a 3kW power generator (working at 40 mA and 45 kV, Cu K α was used as X-Ray source, scan rate selected as 2 $^\circ$ /min) was used. The crystallographic analysis of Electroless B1 and B2 as well as electrolytic Ni coated samples with variable surface metallization processes were done.

The Scherrer calculation was applied to determine the crystal size (a) of the samples after each surface metallization procedures and electrolytic Ni plating. Braggs' law, Gaussian curve fitting and crystallite size calculations were used by given equations Eq. E4-6.

$$n \cdot \lambda = 2 \cdot d \cdot \sin(\theta) \quad (\text{E4})$$

$$y = y_0 + \sqrt{\frac{2}{\pi}} \cdot \frac{A}{B} \cdot e^{-2\left(\frac{x-x_c}{B}\right)^2} \quad (\text{E5})$$

$$a = \frac{K \cdot \lambda}{B \cdot \cos(\theta)} \quad (\text{E6})$$

The shape factor (K) was taken as 1.11 [57,58], Cu K α wavelength (λ) was taken as $1.5406 \cdot 10^{-10}$ m, B is the Full Width Half Maximum (FWHM) of the peak, y_0 an offset of the peak, A the area under the peak, x_c the center of the peak, n a positive integer, θ the glancing angle and d the interplanar distance [59,60].

2.4.2. Electrical Characterization of Metallized PU Surfaces

The electrical properties of PU surfaces after each metallization step were examined in detail in following subsections.

2.4.2.1. Physical Property Measurement System (PPMS) Analysis of Metallized PU Surfaces

The details of measurements are given in section 2.3.2. In order to make a comparison and define the mechanism, PPMS values of neat PU and PU samples after each metallization steps were measured.

CHAPTER 3

RESULTS AND DISCUSSION

3.1. Characterization of a Metallized PU Surface at Each Step

After characterizing neat PU in detail, the characteristics of samples after surface metallization steps and electroless as well as electrolytic Ni plating were observed by microstructural and electrical characterization.

3.1.1. Microstructural Characterization

Surface morphology, surface roughness, XPS and XRD analyses of samples after each metallization step are mentioned briefly in the sections below.

3.1.2. Surface Morphology Analysis

Surface morphology analysis using SEM was applied at each step of surface metallization. The SEM view of sensitized and activated samples with 2000x magnification are given below as Figure 3.1. After sensitization with Sn^{+2} ions, nearly the complete surface of PU was filled with Sn ions, then after the Pd activation process, Pd atoms were nucleated at the surface, the nuclei can be seen below with 5000x magnification as Figure 3.2. The EDS analysis of sensitized and activated samples are shown as Figure 3.3.

There was a small increase of the nuclei of the Pd on the surface of the PdCl_2^* activated sample. The analysis shows that Sn and Pd elements adhere onto the PU surface. However, after Pd sensitization not all Sn atoms are reduced by Pd ions in the electrolyte, which was observed by XPS depicted in Figure 3.12. Another explanation for this result is that the concentration of Pd ions was not high enough for the oxidation of all Sn atoms.

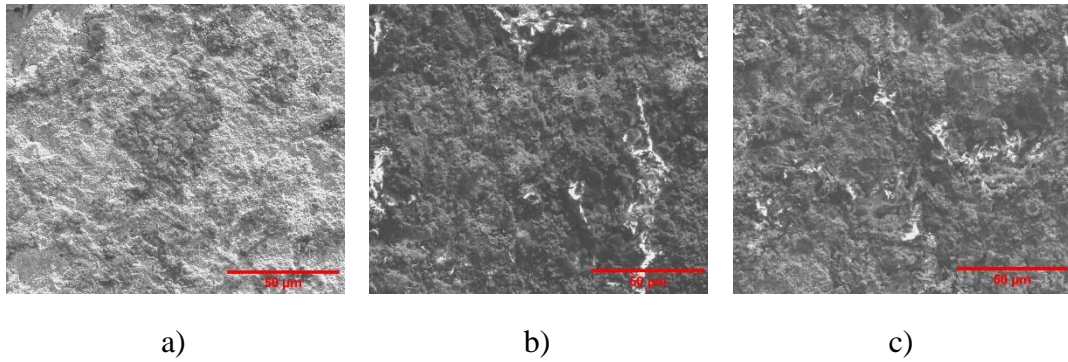


Figure 3.1. The SEM Images of Sensitized and Activated Samples; a) Sn Sensitized, b) PdCl₂ and c) PdCl₂* Activated Samples

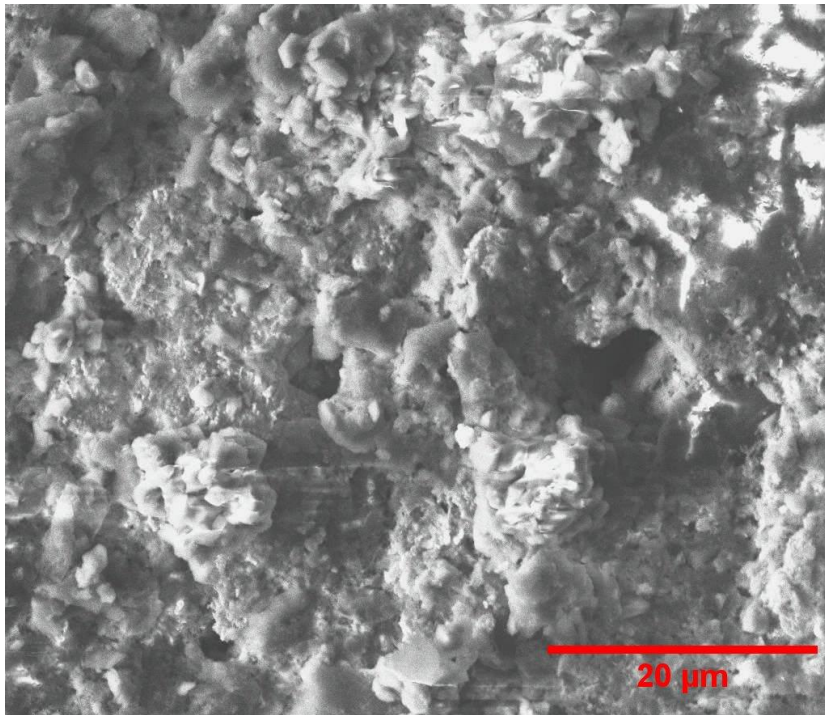
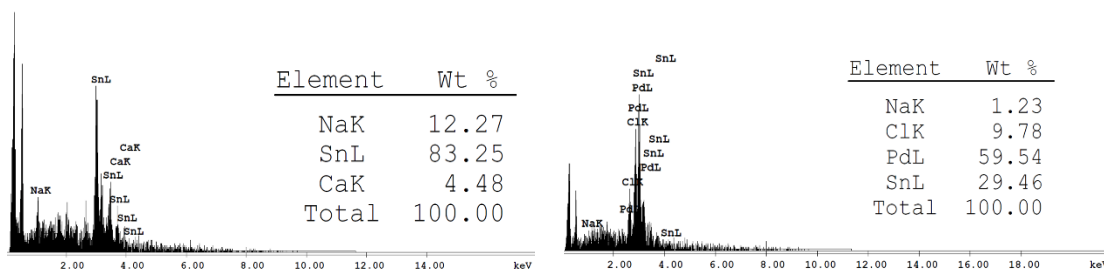


Figure 3.2. Surface Morphology of the PdCl₂* Activated Sample. Note that in this figure the magnification is 5000x. In comparison with the Sn sensitized surface Pd is observable.



a)

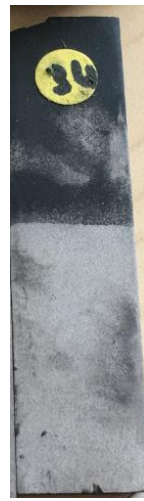
b)

Figure 3.3. EDS Analysis of Sn Sensitized and Pd Activated Samples

After surface metallization, electroless Ni plating was applied both in acidic and alkaline electrolytes. The drastic improvement of the acidic electrolyte on the nucleation sites of Pd elements in contrast to the alkaline electrolyte can be seen even by naked eye as shown in Figure 3.4. Additionally, in the alkaline electrolyte the pH of the solution decreases during the plating process, thus the electrolyte becomes unstable. Due to the instability of the electrolyte, continuity of the process was inhibited, whole nickel ions were reduced at the same time both on substrate and even on other surfaces like the probe, magnetic stir bar and beaker aggressively [61]. This observation is in good agreement with SEM images in Figure 3.5, where the Ni^{2+} ions were reduced on nucleation sites of Pd atoms in a tight manner. Furthermore, the EDS analysis is given as Figure 3.6. Ni^{+2} ions preferred Pd nuclei to be reduced.



a)



b)

Figure 3.4. Images of the Samples Metallized with a) Alkaline and b) Acidic Electrolytes

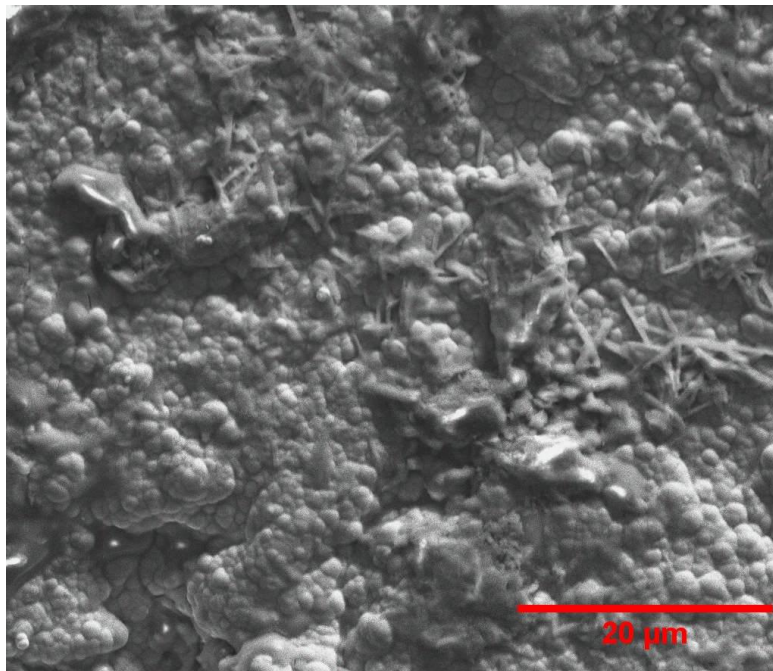


Figure 3.5. Surface Morphology of Acidic Electroless Nickel Electrolyte. Note that in this figure the magnification is 5000x.

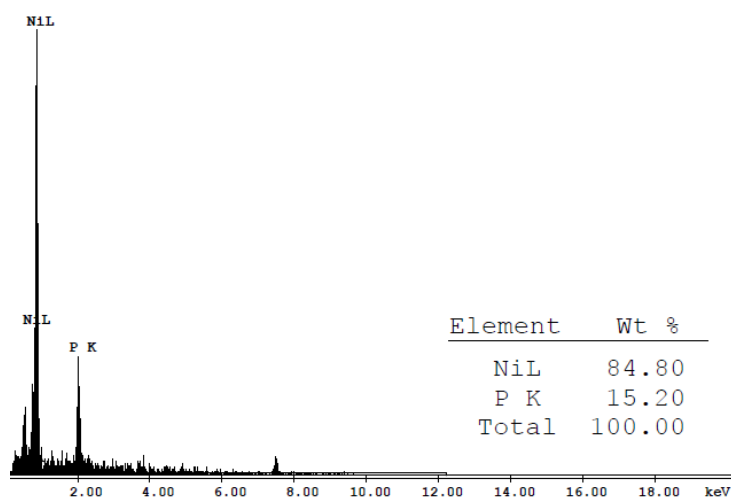


Figure 3.6. EDS Analysis of Acidic Electroless Nickel Plated PU Surface

The change in current efficiencies of the samples were determined by the thickness measured from cross sections of SEM changes. Additionally, the change in the coating weight was measured and compared. Note that, the difference is quite small (see Table 3.1).

The change in current density for each step indicates that the most efficient result was obtained for the B2* sample. Increasing PdCl₂ amount increases the efficiency of Ni atoms to adhere on the surface of the cathode.

First of all, the main purpose of this study was to observe the behavior of each step of the surface metallization and its results on current efficiency. The values calculated from coating thicknesses are given in Table 3.1 below. As seen in Figure 3.7 the influence of the activation process increases the current efficiency drastically. Moreover, the increase in PdCl₂ amount in the activation electrolyte increased the nucleation sites on the surface of the foam and more Ni²⁺ atoms attempted to be reduced.

Secondly, after observation of the effect of the surface activation process and PdCl₂ amount on current efficiency, the behavior of electroless Ni plating on the coating was examined using 2 different coating electrolytes; acidic and alkaline. Nickel plating in the used acidic electrolyte specified in Table 2.2 was a more efficient process than the

B1 (alkaline) electrolyte. The major disadvantage of the basic electrolyte is the plating rate of the process which is approximately 8-10 $\mu\text{m/h}$ [62]. In contrast, the acidic electrolyte with a hypophosphate reducing agent is approximately 25 $\mu\text{m/h}$ [52].

Finally, during these surface metallization processes the current efficiency values were measured at 4 different current density values. Within the framework of this study, the optimized current density value was 3 A/dm^2 . Additionally, the interactions of the PdCl_2 amount and electroless Ni plating baths with respect to current efficiency and current density are given as Figure 3.8.

Table 3.1 *The Current Efficiencies for Each Step*

Surface Metallization Process	Current Density (A/dm^2)	Theoretical Thickness (μm)	Real Thickness (μm)	Current Efficiency (%)
Sn	2	172.2	77.6	45.1
	3	172.2	81.5	47.3
	4	172.2	71.1	41.3
	5	172.2	62.5	36.3
PdCl_2	2	172.2	87.4	50.8
	3	172.2	136.2	79.1
	4	172.2	123.2	71.5
	5	172.2	105.9	61.5
PdCl_2^*	2	172.2	92.1	53.5
	3	172.2	122.7	71.3
	4	172.2	120.4	69.9
	5	172.2	103.2	59.9
B1	2	197.2	138.8	70.4
	3	197.2	159.6	79.8
	4	197.2	112.6	57.1
	5	197.2	123.2	62.5

B1*	2	197.2	156.4	79.3
	3	197.2	159.9	80.9
	4	197.2	157.6	79.9
	5	197.2	144.5	73.3
B2	2	197.2	162.4	82.3
	3	197.2	160.7	81.5
	4	197.2	169.5	85.9
	5	197.2	165.4	83.9
B2*	2	197.2	186.9	94.8
	3	197.2	193.3	98.0
	4	197.2	171.7	87.1
	5	197.2	170.1	86.3

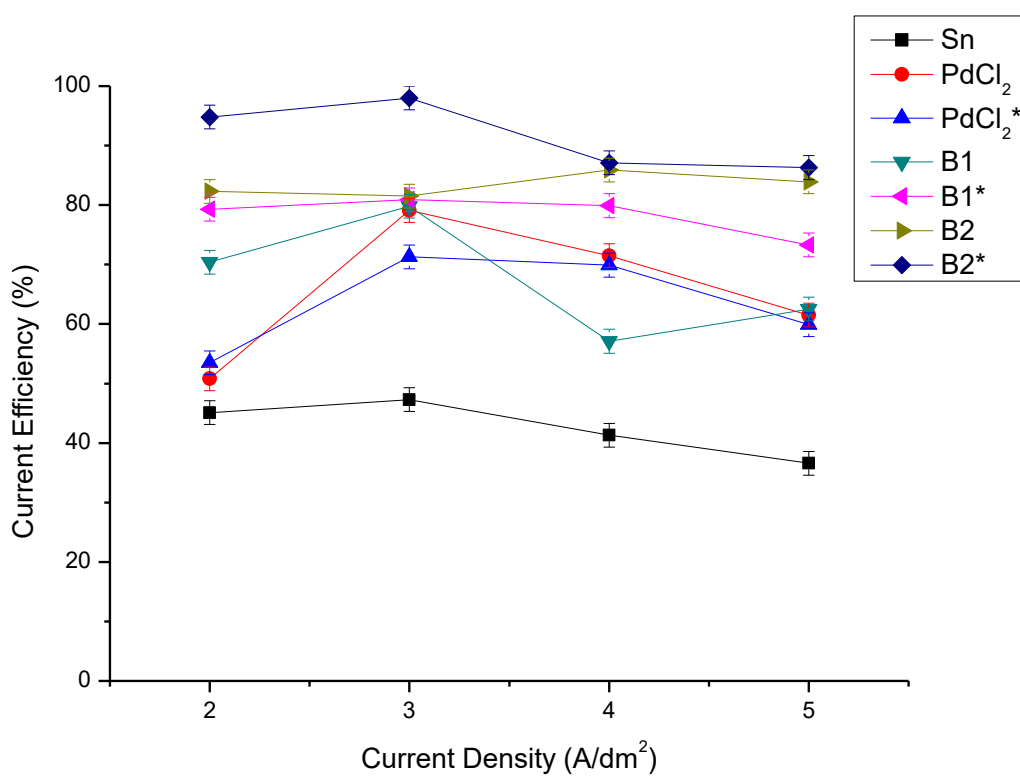


Figure 3.7. Change in Current Efficiencies with respect to Current Densities for Each Surface Metallization Step

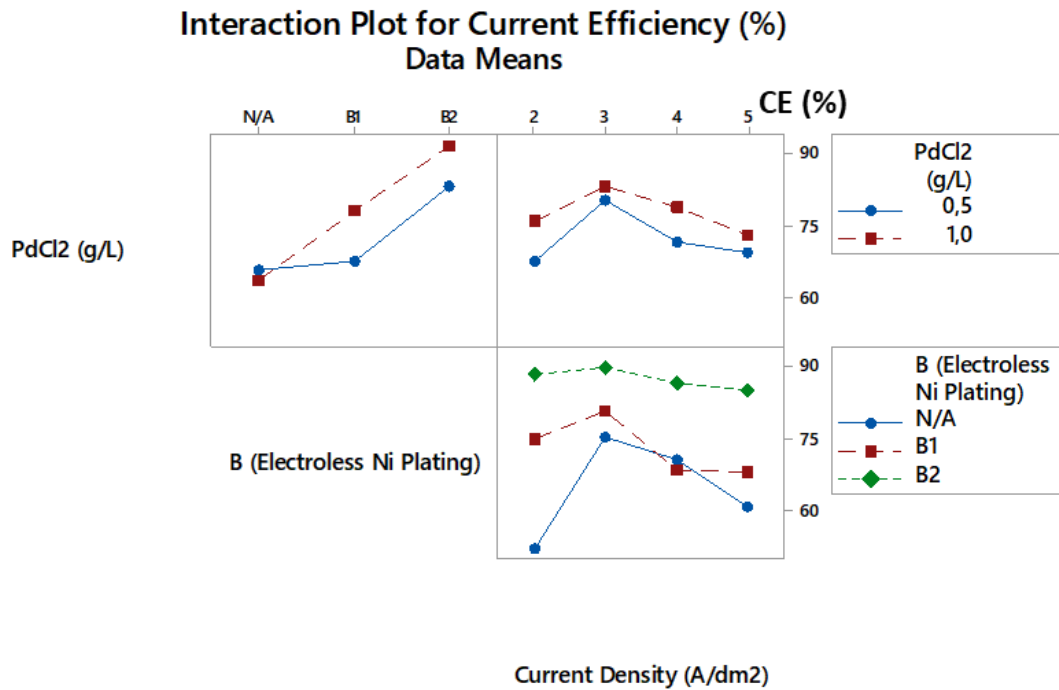


Figure 3.8. Interaction Plot of the Change of Current Density on Current Efficiency for Each Step

As noted above the effects of the PdCl₂ amount, type of electroless Ni plating electrolyte and current density on current efficiency of the electrolytic Ni plating shows parallel results with the main effects plot mentioned in Figure 3.9. This plot shows mean of % current efficiency values for the interaction plot above. The increasing amount of PdCl₂ increases the current efficiency. For the not applicable case of electroless Ni plating, the worst results of current efficiency were observed when compared to the present case. There was a slight increase on the current efficiency after electroless Ni plating in the alkaline electrolyte. However, after electroless Ni plating in the acidic solution, the improvement on the current efficiencies was much more significant than the alkaline plating.

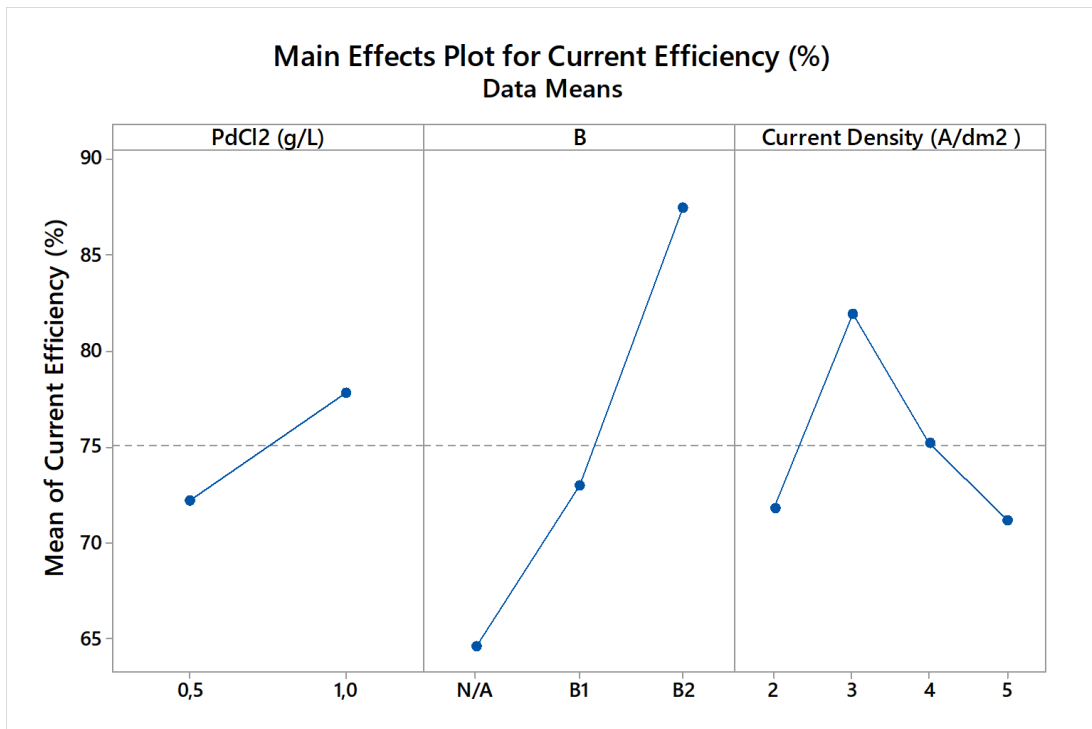


Figure 3.9. Mean Effects Plot of the Change of PdCl₂ Amount, Type of Electroless Ni Plating Electrolyte and Current Density on Current Efficiency for Each Step

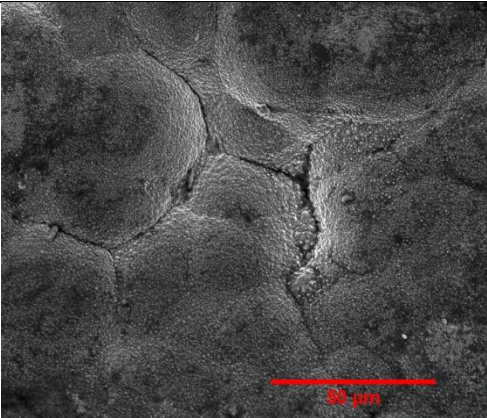
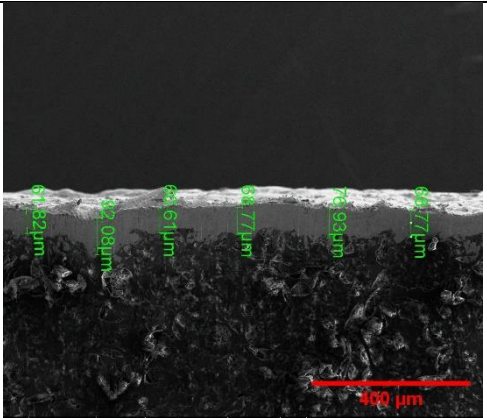
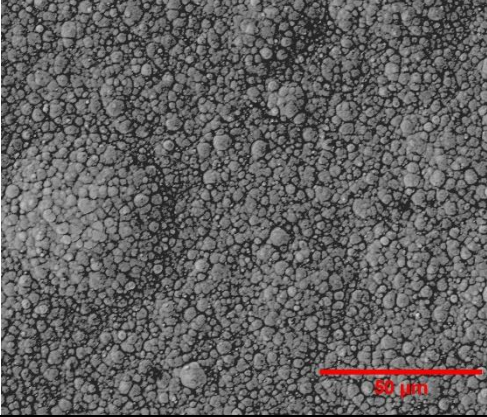
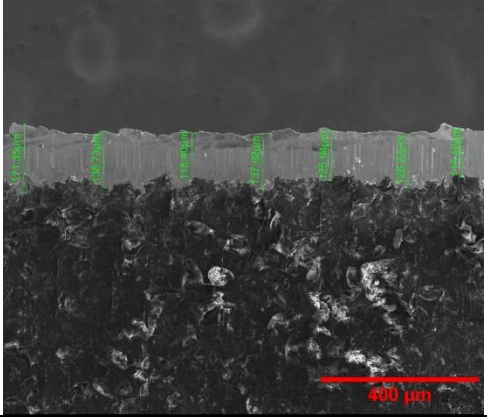
The current efficiency of the coatings was calculated by thicknesses measured from the cross sections of SEM images. The effect of current density on current efficiency indicates the optimum value which is 3 A/dm² and can be seen as an enhancement in Figure 3.7. Each surface metallization process was examined after 172.2 μm theoretical electrolytic Ni plating.

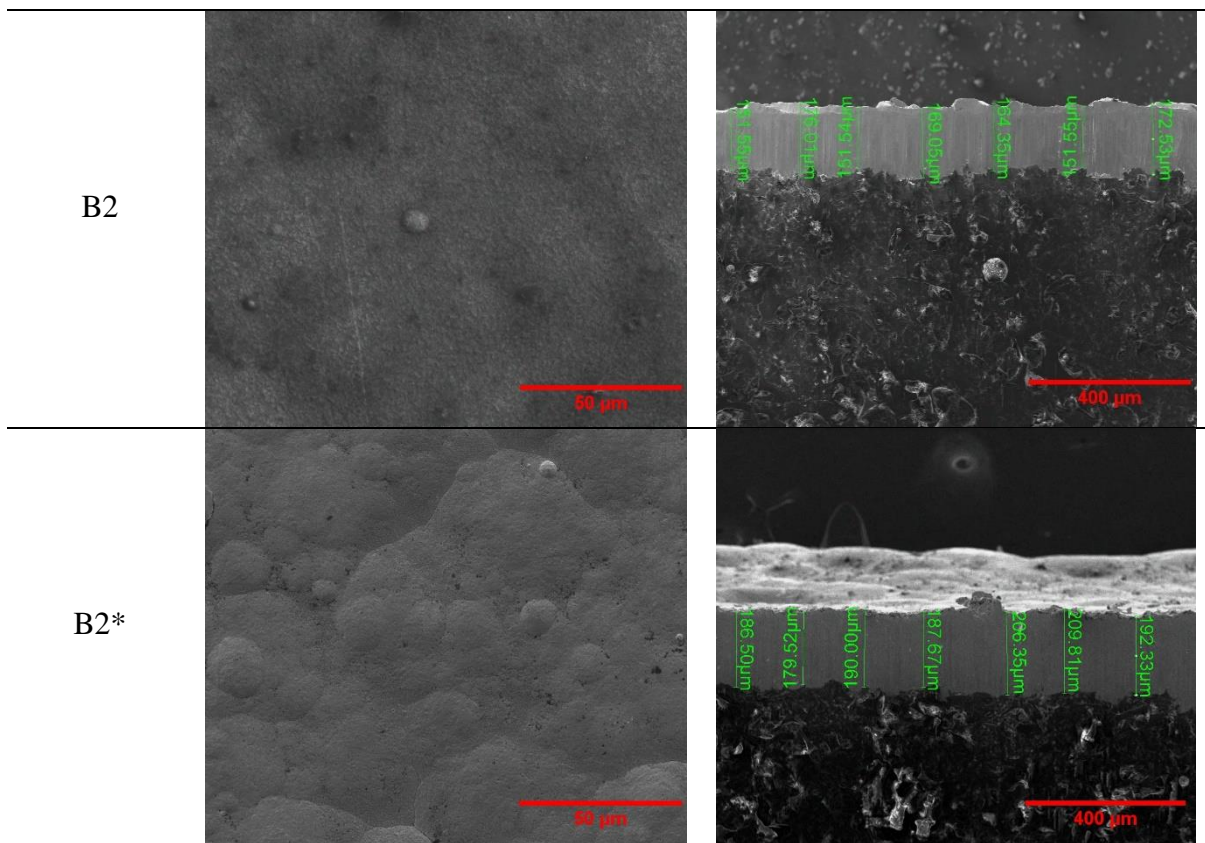
SEM images of electrolytic nickel plated surfaces create under different metallization conditions at different metallization conditions at different current densities are compared in Table 3.2. The surface morphology of the only Sn sensitized sample has the largest grain sizes. The Sn²⁺ ions were located on the surface of PU after the sensitization process. Sn cations act as a scattering center for the electron flow due to its ionization mentioned in subsection 3.1.6.1.

In addition, the smallest grain size was obtained for the sample B2 after sensitization, activation and electroless Ni plating in an acidic electrolyte. The increased amount of

Pd increases the effectiveness of the reducing process of Ni²⁺ ions. These ions are closely packed on the surface. Thus, a finer grain size was obtained. Moreover, the subsequent surface metallization process improves the surface quality and yields finer grain sizes. Better results were obtained from acidic rather than alkaline electrolyte.

Table 3.2. The SEM Views of Electrolytic Ni Plated Surfaces with a Current Density of 3 A/dm²

Surface Metallization Process	SEM Microview of 3 A/dm ² Plated Samples	Cross- Section SEM Microview of 3 A/dm ² Plated Samples
Sn		
PdCl ₂		



3.1.3. Surface Roughness Measurement

The surface roughness measurements were performed by the profilometer before and after electrolytic Ni deposition (see Fig. 3.10). There is a significant increase of surface quality of the coatings on PU foam after electrolytic Ni plating with variable current densities (2, 3, 4, 5 A/dm²). The position of scanned regions (left, middle and right) by profilometer show a slight difference in the surface quality. On the other hand, the surface smoothness increased before and after the electrolytic Ni plating of the substrate. Especially for electrolytic Ni deposition at 3 A/dm² current density, the change in surface roughness is higher than the other cases. Observable improvement on the surface roughness before and after electrolytic nickel plating at 3 A/dm² is in accord with the SEM micro views and show good agreement.

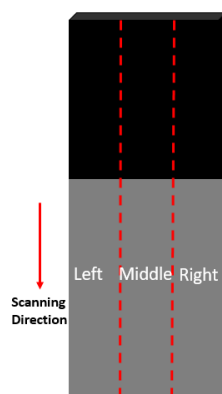


Figure 3.10. Scan Direction and the Scanning Areas of Nickel Plated PU Foam

After the grinding process, the surface roughness of PU was decreased within the range 1.5 to 2 μm . The effects of the PdCl_2 amount, type of electroless Ni plating electrolyte and applied current densities (2, 3, 4, 5 A/dm^2) on the surface roughness of the substrate was examined and seen in Figure 3.11. Increasing the amount of PdCl_2 in the activation solution slightly increase the surface roughness. This increase can be the result of the inhomogeneous distribution of Pd clusters on the substrate. The acidic electroless Ni plating electrolyte yields improved surface quality of the coating by reducing the bulk resistivity of the surface. After the acidic electroless Ni plating procedure, the surface of the substrate was fully metallized and the smallest grain size was obtained. Decreasing the grain size improves the surface quality of the coating and decreases the surface roughness. Moreover, the smallest surface roughness value was obtained at 3 A/dm^2 current density.

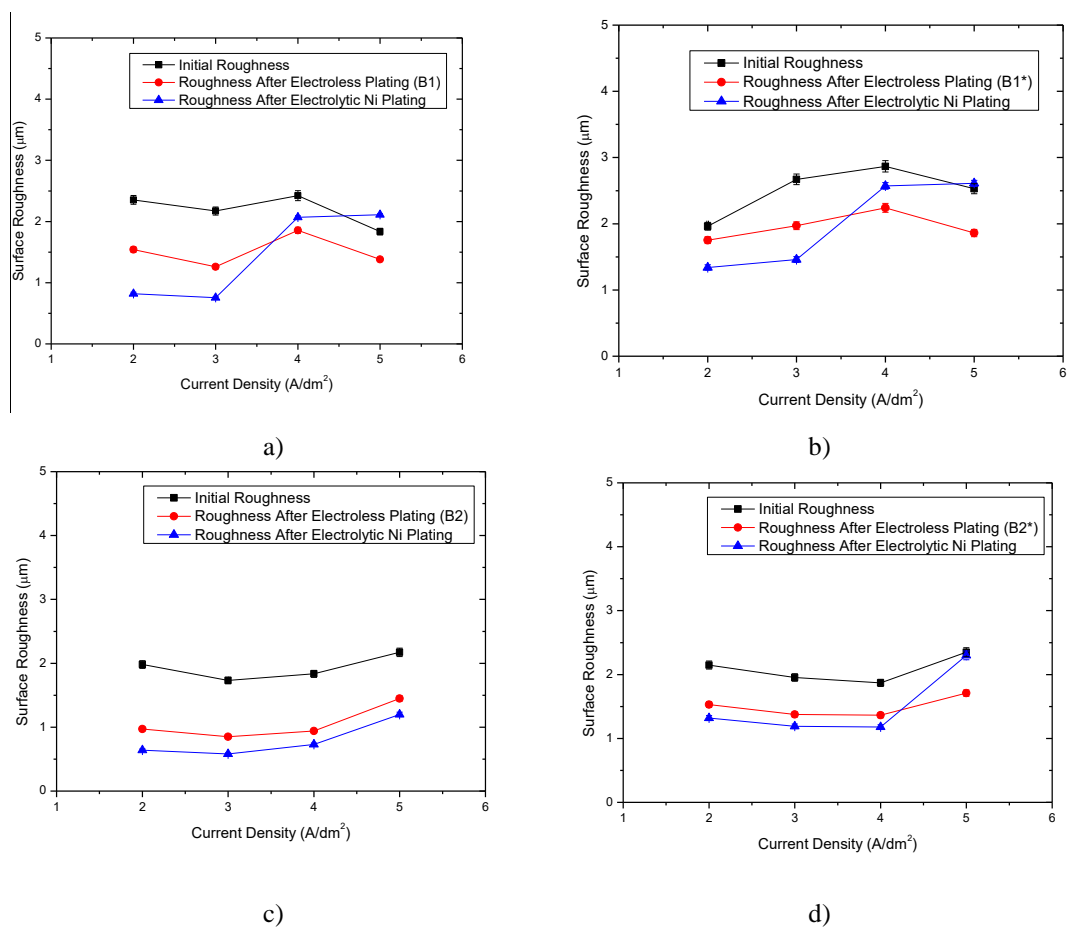


Figure 3.4. The Change in the Surface Roughness of the PU Substrate a) After Alkaline Electroless Ni Plating with 0.5 g/L PdCl₂ and b) 1 g/L PdCl₂ Activation Solution c) After Acidic Electroless Ni Plating with 0.5 g/L PdCl₂ and d) 1 g/L PdCl₂ Activation Solution

3.1.4. XPS Analysis

XPS analyses were applied to each surface of metallization step, electroless and electrolytic plating and the cross sections of plated PU foams. The chemical compositions of the surfaces up to 10 nm depth were examined and it was aimed to evaluate the surface metallization mechanism. As seen in Figure 3.12., the peaks of the elements on the surface of the only Sn sensitized sample are Na, Sn and Cl. During the surface cleaning process by the alkaline solution NaOH, Na₂CO₃, Na₃PO₄ compounds were used to clean its surface from dirt and grease. Thus, the Na peak is expected since the substrate material is high density foam and it absorbs the alkaline

solution. Additionally, the chlorine peak is coming from HCl in the surface sensitization solution. After the surface sensitization, an activation process was applied to oxidize Sn^{2+} ions to Sn^{4+} and reduce Pd^{2+} ions to Pd atoms. The observed peaks after the activation with solutions containing PdCl_2 in amounts of both 0.5 and 1 g/L are Na, Sn, Pd, Cl and P sourced. Na and P peaks are probably coming from the surface cleaning procedure and the chlorine peak is observed because of HCl in the activation solution. It is quite surprising that Sn^{2+} ions are present even after Pd activation. This Sn peaks indicate that some of the Sn^{2+} ions were not oxidized after immersion in the activation solution. After sensitization and activation, the surface was metallized with electroless Ni plating. Regardless of the type of the electrolyte, Sn peaks are observed after electroless Ni plating due to the porous nature of PU. Unstable Sn^{2+} ions stay still in the foam. Since XPS measurements are taken in a vacuum environment, Sn peaks are still visible. However, the surface of the foam was rinsed, vacuumed and rinsed again after the activation process. In this way, the amount of Sn on the surface of the foam decreased below 1 atomic %.

Furthermore, after electroless Ni plating, Pd peaks disappear and this behavior indicates that all of the reduced Pd atoms act as a reduction site for Ni^{2+} ions to reduce on the cathode. In addition, after alkaline electroless Ni plating, Na and P peaks are also observed along with Sn and Ni peaks. As mentioned above Na peak can be residual of alkaline cleaning treatment and the source of P peak is the hypophosphite reducing agent in the electroless Ni plating electrolyte. For the acidic electroless Ni plating case, an additional S peak is observed. This peak might occur because of the nickel sulphate in the acidic electroless Ni plating electrolyte. Furthermore, Sn peaks are still present after electrolytic Ni plating at the cross section of the sample and even on the surface of the electrolytic Ni plating.

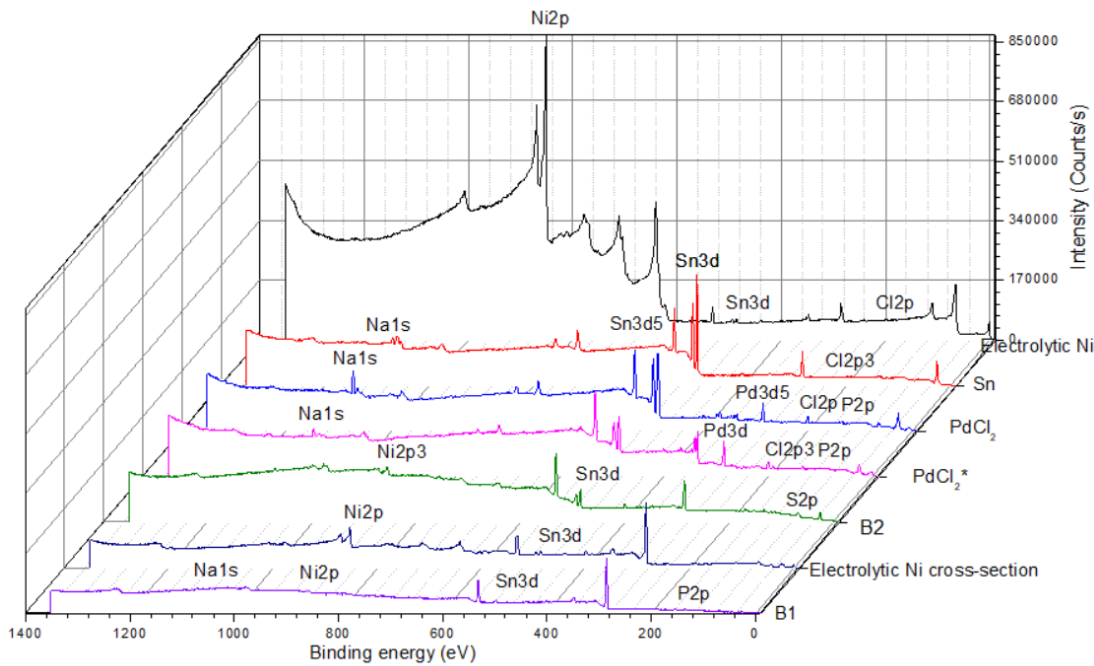


Figure 3.5. XPS Analysis of Each Sample. Note the Sn3d5 peak which indicates the presence of Sn⁴⁺ for the PdCl₂ sample and the high Sn3d peak for the Sn sample which shows that Sn²⁺ does not oxidize completely [71].

3.1.5. XRD Analysis

The position of diffraction peaks and the d-spacings that they represent provide information about the location of lattice planes in the crystal structure. Each peak measures a d-spacing that represents a family of lattice planes.

XRD analysis was applied for electroless and electrolytic Ni plated samples after each step. As seen in Figure 3.13, the peaks of pure FCC Ni are observed in all diffractions. The highest peak from (200) reflection common for all diffractions indicate the preferred orientation of texture at 3 A/dm² current density.

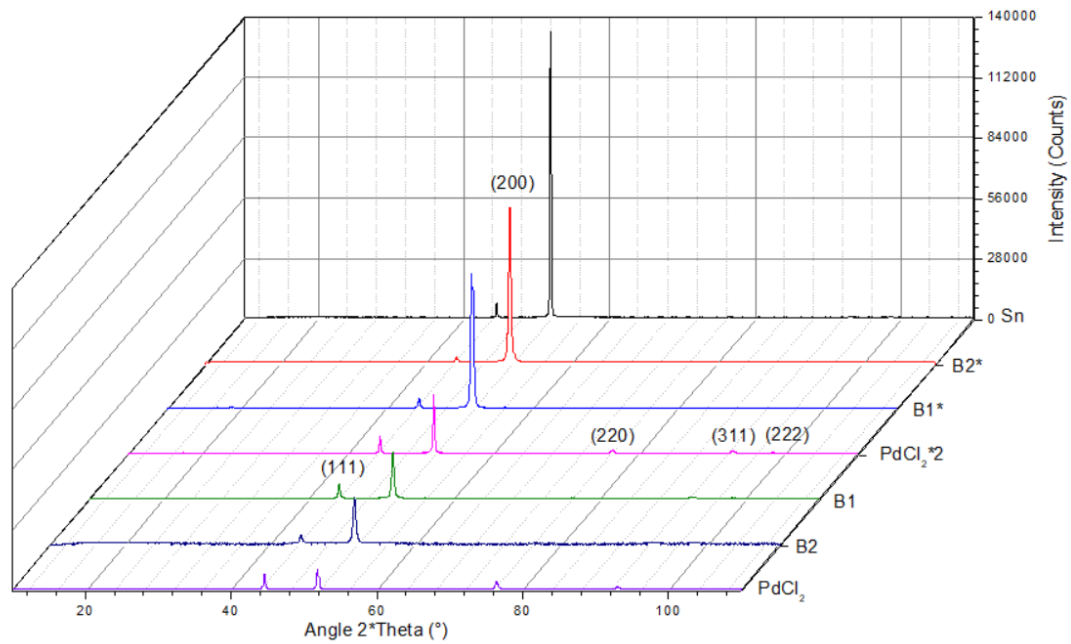


Figure 3.6. XRD Analysis of Each Sample

Use of Scherrer equation (Eq. E6) yields the mean ordered crystallized domain size, which is a minimum for the grain size of the coating. SEM images in Table 3.2 indicate large grain sizes especially for only Sn sensitized and electrolytic Nickel coated samples. This observation is in good agreement with the analysis by Scherrer equation whose results are given in Table 3.3 and Figure 3.14. Nevertheless, it should be noted that the grain sizes of the only Sn sensitized samples is quite large and lies above the quantitative limit of Scherrer's equation [74-76]. Therefore, in this case the crystallite size should be interpreted qualitatively. In addition, considering the values as well as its errors (Δa) calculated by propagation of Gaussian uncertainty yields more or less the same mean ordered crystallized domain size for all samples except the Sn sensitized and electrolytic Nickel coated sample. Comparison of the absolute values shows a discrepancy of at least 200% between the alkaline electroless Ni plated sample and the exceptional one.

Table 3.3. Scherrer Calculation for each Surface Metallization Process

Surface Metallization Process	B (FWHM)	ΔB	θ	$\Delta\theta$	a (m)	Δa (m)
Sn	0.00104	2.42 E-05	0.453	1.32 E-05	1.83 E-07	4.25 E-09
PdCl ₂	0.00302	2.09 E-05	0.451	8.90 E-06	6.28 E-08	4.35 E-10
PdCl ₂ *	0.00263	1.99E-05	0.453	8.15 E-06	7.24 E-08	5.51 E-10
B1	0.00207	3.26 E-05	0.453	1.24 E-05	9.16 E-08	1.44 E-09
B1*	0.00285	2.02 E-05	0.450	6.19 E-06	6.66 E-08	4.71 E-10
B2	0.00365	3.05 E-05	0.451	1.12 E-05	5.20 E-08	4.33 E-10
B2*	0.00212	3.7 E-05	0.454	1.11 E-05	8.97 E-08	1.56 E-09

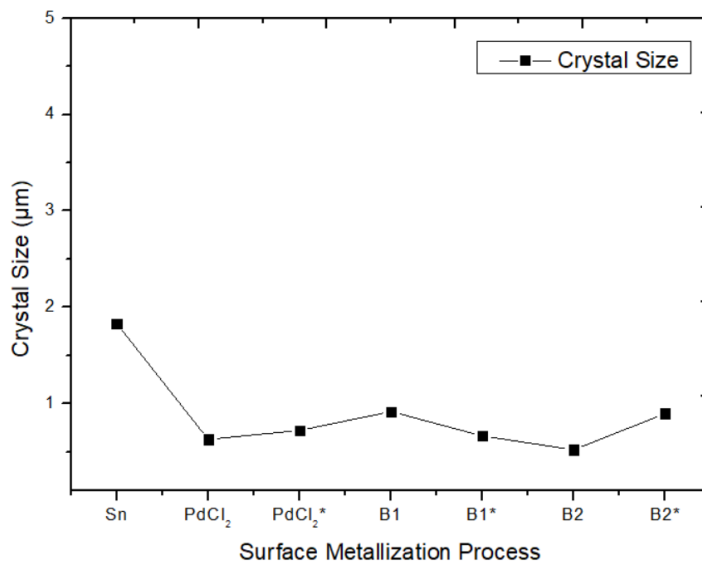


Figure 3.7. The Change in the Crystallite Size with respect to the Surface Metallization Process

3.1.6. Electrical Characterization

In the following subsection the results of the PPMS measurements are summarized.

3.1.6.1. Physical Property Measurement System (PPMS) Analysis

The change of the bulk resistivity with respect to the temperature of the samples, which represented the different experimental steps are given below as Figure 3.15 and Figure 3.16. It was seen that Sn^{+2} ions diffused into the pores of the foam and act as ionized impurities after the surface sensitization process. It is well known that this can lead to a scattering of charge carriers in the sample [63,69], which means that a drop of the conductivity might occur in such a case. This effect was observed and can be seen in Figure 3.15.

Principally, there are two types of relevant scatterings in our case; the typically occurring lattice scattering and the mentioned ionized impurity scattering, which can be analyzed by use of the Rutherford scattering formula [64]. Coulomb interaction leads to elastic scattering of charged particles. Note that Rutherford's results were historically used for the development of an atom model. However, the formula itself can also be applied in this study [65]. The ionized impurity effect can be seen only for cations, while charge neutral atoms don't show such a behavior [66]. Note that this effect was also observed for other polymers [70].

Pd atoms reduce on the substrate after the activation step and Sn^{2+} ions oxidize to Sn^{4+} and dissolve into the solution. Hence, the ionized impurity effect was not observed. Thus, the following PPMS characterization results show the decreasing trend of bulk resistivity values except for the Sn case.

Additionally, the variation of electrical resistivity of PdCl_2 activated samples are shown in Figure 3.16. The reason for this vibration may be due to the non-homogenous Pd nuclei, and this non-homogeneity continues for electroless Ni plated samples. Moreover, the electrical behavior of PU was not affected much after the alkaline electroless plating using B1.

As expected the sample with the smallest bulk resistivity is electrolytic Ni plated PU. The most effective surface metallization step is determined as sensitization, 1 g/L PdCl_2 activation and electroless Ni plating in an acidic electrolyte. The resistivity

value of this sample is approximately $0.06 \Omega \cdot m$. Besides, the electrolytic Ni plated sample has the lowest bulk resistivity which is nearly $0.002 \Omega \cdot m$. Furthermore, the results of all samples tend to increase by raising temperature, which is expected. Temperature change affects the vibrations of the atoms. Hence, the increased vibration of atoms prevents the current to flow [67].

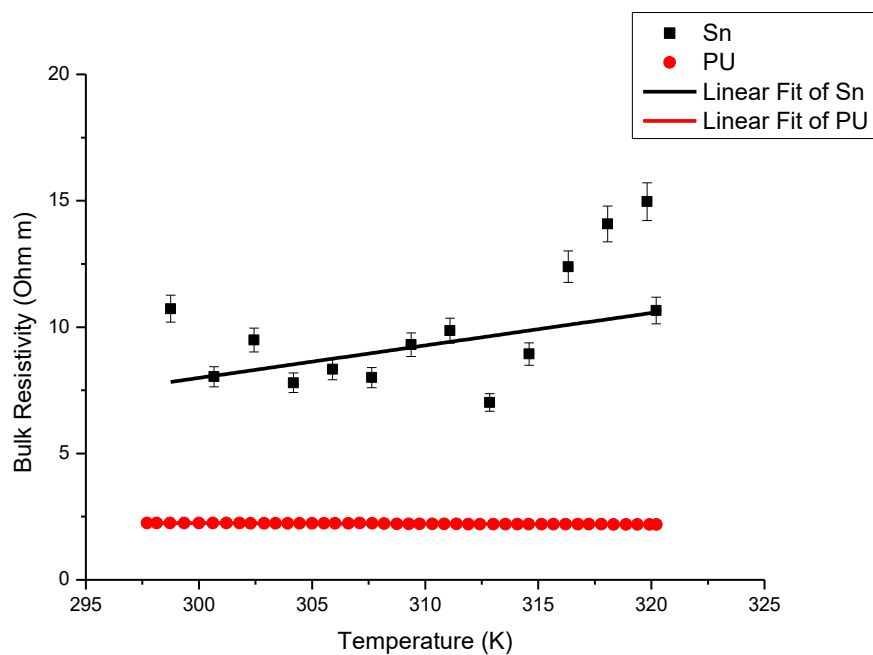


Figure 3.8. The PPMS Measurement of Sn Sensitized Sample in Contrast to Neat PU

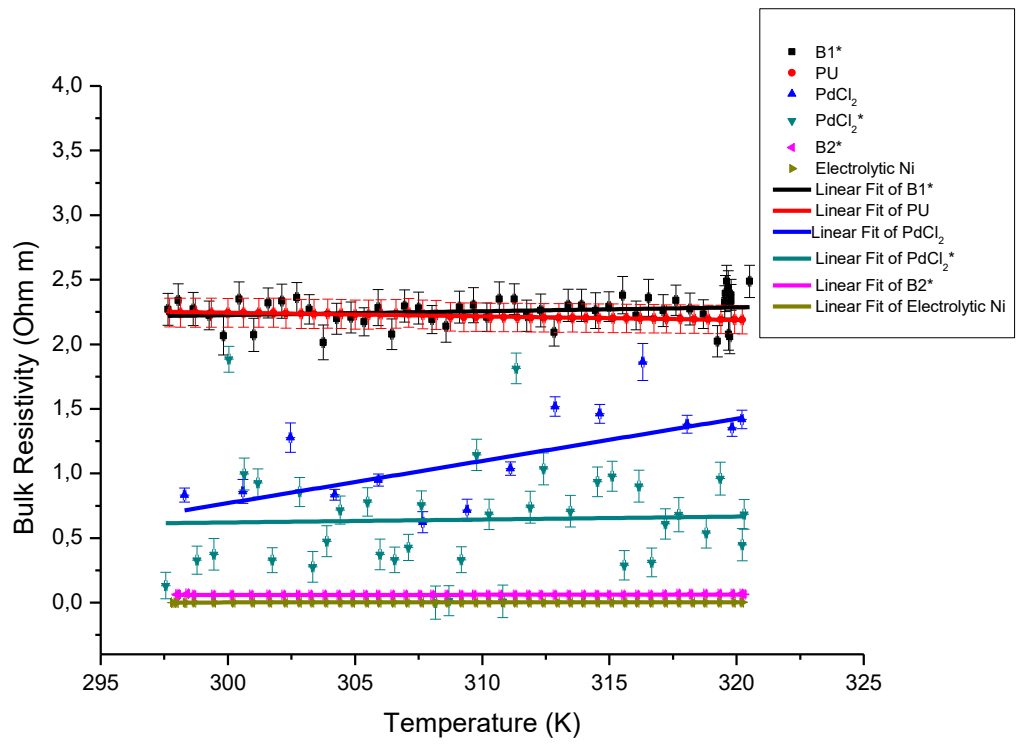


Figure 3.9. The PPMS Measurement of Metallized Samples

CHAPTER 4

CONCLUSION

The measurement of the linear coefficient of thermal expansion of neat PU shows insignificant expansion up to approximately 85 °C. Thermal degradation starts at approximately 220 °C. Additionally, surface roughness of grinded PU was within the acceptable range i.e. 0.9-1 µm. The bulk resistivity of neat PU is approximately 2.2 $\Omega \cdot m$.

Surface morphology analysis after surface metallization procedures indicates that the increasing Pd amount in the surface activation electrolyte increases the current efficiency. The other important effect on surface metallization was the electroless Ni plating. The increasing influence on current efficiency and the conductivity of the surface of PU was obtained by using electroless Ni plating in an acidic electrolyte. The SEM microviews of samples showed that finer grains were obtained at 3 A/dm² current density. Moreover, the surface roughness analysis showed parallel results. The lowest surface roughness value which is approximately 0.6 µm was obtained from acidic electroless Ni plated samples.

Furthermore, elemental analysis of each step of the surface metallization was performed by use of XPS. The most surprising result was the detection of Sn peaks after each metallization step. The reason for this behavior is probably the presence of non-adherent Sn²⁺ ions on the surface of the foam regardless of the type of the electrolyte.

Moreover, XRD analysis was applied after each step. FCC Ni peaks were observed. The highest peak from (200) reflection common for all diffractions indicate preferred orientation of texture at 3 A/dm² current density.

The electrical resistivity value of the electroless Ni plated sample in an acidic electrolyte is approximately $0.06 \Omega \cdot m$. Besides, the electrolytic Ni plated sample has the lowest bulk resistivity which is nearly $0.002 \Omega \cdot m$.

To sum up, it is necessary to follow the steps; Sn sensitization, 1 g/L PdCl₂ containing surface activation, electroless Ni plating in an acidic electrolyte and electrolytic Ni plating at 3 A/dm² current density for production of a Ni lay-up tool.

REFERENCES

- [1] Maria, M. (2013). Advanced composite materials of the future in aerospace industry. *Incas Bulletin*, 5(3), pp. 139–150. <https://doi.org/10.13111/2066-8201.2013.5.3.14>
- [2] Rana, S., & Fanguerio, R. (2016). *Advanced composites in aerospace engineering* (pp. 1–15). pp. 1–15. Retrieved from <http://dx.doi.org/10.1016/B978-0-08-100037-3.00001-8>
- [3] Kamali, G. (2017a). Advanced Composite Materials of the Future in Aerospace Engineering. *International Journal for Research in Applied Science and Engineering Technology*, pp. 610–614. <https://doi.org/10.22214/ijraset.2017.2091>
- [4] Mangalgi, A. D. A. (1999). Composite materials for aerospace applications. *Bulletin of Material Science*, 22(3), pp. 657–664.
- [5] Balakrishnan, P., John, M. J., Pothan, L., Sreekal, M. S., & Thomas, S. (2016). *Natural fibre and polymer matrix composites and their applications in aerospace engineering* pp. 365–383. <https://doi.org/http://dx.doi.org/10.1016/B978-0-08-100037-3.00012-2>
- [6] Meola, C., Boccardi, S., & Carlomagno, G. maria. (2017). Composite Materials in the Aeronautical Industry. *Infrared Thermography in the Evaluation of Aerospace Composite Materials*, pp. 1–24. <https://doi.org/10.1016/b978-1-78242-171-9.00001-2>
- [7] Harris, C., J.H., S., & Shuart, M. J. (2002). *Design and Manufacturing of Aerospace Composite Structures, State-of-the-Art Assessment* pp. 545–560.
- [8] Li, Y., Li, N., & Gao, J. (2014). Tooling design and microwave curing technologies for the manufacturing of fiber-reinforced polymer composites in aerospace applications. *International Journal of Advanced Manufacturing Technology*, 70(1–4), pp. 591–606. <https://doi.org/10.1007/s00170-013-5268-3>
- [9] Kappel, E., Stefaaniak, D., & Hühne, C. (2013). Process distortions in prepreg manufacturing – An experimental study on CFRP L-profiles. *Composite Structures*. pp. 615–625.
- [10] Golzar, M., & Poorzeinolabedin, M. (2010). Prototype fabrication of a composite automobile body based on integrated structure. *International Journal of Advanced Manufacturing Technology*, Vol. 49, pp. 1037–1045. <https://doi.org/10.1007/s00170-009-2452-6>

- [11] Abberger, S.L. (1989). Advanced composite moulds-a new use for invar. *Journal of Chemical Information and Modeling*, 53, pp. 160. <https://doi.org/10.1017/CBO9781107415324.004>
- [12] Wimpenny, D. I., & Gibbons, G. J. (2003). *Metal spray tooling for composite forming* . pp. 443–448. [https://doi.org/10.1016/S0924-0136\(03\)00114-6](https://doi.org/10.1016/S0924-0136(03)00114-6)
- [13] Smith, R.; Lewis, G.; Yates, D. (2001). Development and application of nickel alloys in aerospace engineering. *Aircraft Engineering and Aerospace Technology*, 73(2), pp. 138–146.
- [14] Mott, N. F. (1949). Mechanical properties of metals. In *Physica* (7th ed., Vol. 15). [https://doi.org/10.1016/0031-8914\(49\)90034-8](https://doi.org/10.1016/0031-8914(49)90034-8)
- [15] Corbacho, J.L., Suárez, J. C., & Molleda, F. (2010). Welding of Invar Fe-36Ni alloy for tooling of composite materials, *Welding International*. pp. 966–971. Retrieved from <https://www.tandfonline.com/loi/twld20>
- [16] Boey, F. Y. C., & Lee, W. L. (1990). Microwave radiation curing of a thermosetting composite. *Journal of Materials Science Letters*. <https://doi.org/10.1007/BF00721880>
- [17] Jasthi, B. K., Arbegast, W. J., & Howard, S. M. (2009). Thermal expansion coefficient and mechanical properties of friction stir welded invar (Fe-36%Ni). *Journal of Materials Engineering and Performance*, Vol. 18, pp. 925–934. <https://doi.org/10.1007/s11665-008-9320-7>
- [18] Corbacho, José L., Suárez, J. C., & Molleda, F. (1998). Grain Coarsening and Boundary Migration during Welding of Invar Fe-36Ni Alloy. *Materials Characterization*, Vol. 41, pp. 27–34. [https://doi.org/10.1016/s1044-5803\(98\)00020-5](https://doi.org/10.1016/s1044-5803(98)00020-5)
- [19] *Molding Methods & Tooling*. (1990). Retrieved from <https://www.aircraftspruce.com/catalog/pdf/13-18000.pdf>
- [20] Miller, F. B., Benne, M. E., & Dull, K. (2010). *Leak Detection In Composite Tools Inventors*. US: United States Patent Application Publication.
- [21] Lucas, R., & Danford, H. (2009). Case studies: Low cost, high-strength, large carbon foam tooling. *SAMPE Journal*, Vol. 45, pp. 20–28.
- [22] Jordan, L., & Swanger, W. H. (2012). The properties of pure nickel. *Bureau of Standards Journal of Research*, 5(6), pp. 1291. <https://doi.org/10.6028/jres.005.075>
- [23] Pervaiz, S., Rashid, A., Deiab, I., & Nicolescu, M. (2014). *Influence of Tool Materials on Machinability of Titanium- and Nickel-Based Alloys: A Review [23].pdf* (pp. 219–252). pp. 219–252. <https://doi.org/10.1080/10426914.2014.880460>

- [24] Lee, C. K. (2009). Structure, electrochemical and wear-corrosion properties of electroless nickel-phosphorus deposition on CFRP composites. *Materials Chemistry and Physics*, 114(1), pp. 125–133. <https://doi.org/10.1016/j.matchemphys.2008.08.088>
- [25] Rose, I., & Whittington, C. (2014). *Nickel Plating Handbook*. Retrieved from www.nickelinstitute.org
- [26] Hernández, P., Campos, D., Soccoro, P., Benítez, A., Ortega, F., Diaz, N., & Marrero, M. D. (2015). *Procedia Engineering*, Vol. 132. pp. 655–662. <https://doi.org/10.1016/j.proeng.2015.12.544>
- [27] MacGeough, J. A., Leu, M. C., Rajurkar, K. P., De Silva, A. K. M., & Liu, Q. (2001). Electroforming process and application to micro/macro manufacturing. *CIRP Annals - Manufacturing Technology*, Vol. 50, pp. 499–514. [https://doi.org/10.1016/S0007-8506\(07\)62990-4](https://doi.org/10.1016/S0007-8506(07)62990-4)
- [28] Keresztes, R., Kalácska, G., Zsidai, L., & Dobrocsi, Z. (2011). Machinability of engineering polymers. *Sustainable Construction and Design*.
- [29] Logie, G. R., & Rantell, A. (1968). The Adhesion of Electroless Metal Deposits to A B S and other Polymers. *Transactions of the IMF*, 46(1), pp. 91–94. <https://doi.org/10.1080/00202967.1968.11870055>
- [30] Arrowsmith, D. J. (1970). Adhesion of Electroformed Copper and Nickel to Plastic Laminates. *Transactions of the IMF*, 48(1), pp. 88–92. <https://doi.org/10.1080/00202967.1970.11870136>
- [31] Warfield, R. W., & Petree, M. C. (1961). Electrical Resistivity of Polymers. *SPE Transactions*.
- [32] Mallory, G. O., & Hajdu, J. B. (1990). Chapter 1 The Fundamental Aspects Of Electroless Nickel Plating. *Electroless Plating - Fundamentals and Applications*, pp. 1–56.
- [33] Yang, W., Luo, S., Zhang, B., Huang, Z., & Tang, X. (2008). Electroless preparation and characterization of magnetic Ni-P plating on polyurethane foam. *Applied Surface Science*, 254(22), pp. 7427–7430. <https://doi.org/10.1016/j.apsusc.2008.05.343>
- [34] Fujii, S., Hamasaki, H., Takeoka, H., Tsuruoka, T., Akamatsu, K., & Nakamura, Y. (2014). Electroless nickel plating on polymer particles. *Journal of Colloid and Interface Science*, 430, 47–55. <https://doi.org/10.1016/j.jcis.2014.05.041>
- [35] Bergström, E. A. (1955). Surface Metallizing Method. *U.S. Patent Office*. <https://doi.org/10.1126/science.53.1377.481>
- [36] Bergström, E. A. (1971). Process For Purfying A Metal Layer Is True At High Ph Values. Precipitated Catalytically Onto A It Is Known To Treat Precipitated

Metal Catalysts At Ele Carrier Of Glass, Ceramic, Metal Or. *United States Patent Office*.

- [37] Marton, J. P., & Schlesinger, M. (1968). The Nucleation, Growth, and Structure of Thin Ni-P Films. *Journal of the Electrochemical Society*, 115(1), pp. 16–21. <https://doi.org/10.1149/1.2410991>
- [38] Seko, A., Togo, A., Oba, F., & Tanaka, I. (2008). Structure and stability of a homologous series of tin oxides. *Physical Review Letters*, 100(4), pp. 2–5. <https://doi.org/10.1103/PhysRevLett.100.045702>
- [39] Cohen, A. R. L. (2016). Mössbauer Spectroscopy: Recent Developments *Published by: American Association for the Advancement of Science Stable URL: http://www.jstor.org/stable/1734900 JSTOR is a not-for-profit service that helps scholars, researchers, and students discover, 178(4063), pp. 828–835.*
- [40] Waard, H., & Cohen, R. L. (1974). pp. 3760–3774. *Physical Review B*, 10(9), pp. 3760-3774.
- [41] Cohen, R. L., D'Amico, J. F., & West, K. W. (1971). Mössbauer Study of Tin(II) Sensitizer Deposits on Kapton. *Journal of the Electrochemical Society*, 118(12), 2042–2046. <https://doi.org/10.1149/1.2407909>
- [42] Schlesinger, M. (2011). Electroless Deposition of Nickel. *Modern Electroplating: Fifth Edition*, 4(3), pp. 447–458. <https://doi.org/10.1002/9780470602638.ch18>
- [43] Meek, R. L. (1975). A Rutherford Scattering Study of Catalyst Systems for Electroless Cu Plating: II. SnCl₂ Sensitization and PdCl₂ Activation. *Journal of the Electrochemical Society*, 122(11), pp. 1478–1481. <https://doi.org/10.1149/1.2134045>
- [44] Brenner, A., & Riddell, G. E. (1946). Nickel plating on steel by chemical reduction. *Journal of Research of the National Bureau of Standards*, 37(1), pp. 31. <https://doi.org/10.6028/jres.037.019>
- [45] Krishnan, K. H., John, S., Srinivasan, K. N., Praveen, J., Ganesan, M., & Kavimani, P. M. (2006). An overall aspect of electroless Ni-P depositions—A review article. *Metallurgical and Materials Transactions A*, 37(6), 1917–1926. <https://doi.org/10.1007/s11661-006-0134-7>
- [46] Goldie, W. (1968). Metallic Coating of Plastics. *British Isles: Electrochemical Publications Ltd*.
- [47] Song, Y. W., Shan, D. Y., & Han, E. H. (2008). High corrosion resistance of electroless composite plating coatings on AZ91D magnesium alloys. *Electrochimica Acta*. <https://doi.org/10.1016/j.electacta.2007.09.026>
- [48] Parkinson, R. (1997). Properties and Applications of Electroless Nickel. *Nickel Development Institute Publication*, pp. 33. Retrieved from

http://www.nickelinstitute.org/TechnicalLiterature/TechnicalSeries/PropertiesandApplicationsofElectrolessNickel_10081_.aspx

- [49] Schafer, R. A., Mohler, J. B., & Pochapsky, H. (1950). Apparatus for Plating, United States Patent Office.
- [50] Popov, K., Djokic, S. S., & Grgur, B. N. (2002). Fundamental Aspects of Electrometallurgy. *Chapter 2 Definitions, Principles and Concepts*. <https://doi.org/10.1007/b118178>
- [51] Parkinson, R. (1999). Electroforming: a unique metal fabrication process. *AIFM Galvano Tecnica e Nuove Finiture(Italy)*, 9(3), pp. 140–142. Retrieved from http://www.nickelinstitute.org/~Media/Files/TechnicalLiterature/Electroforming_AUniqueMetalFabricationProcess_10084_.pdf
- [52] Nunes, R. M., U., Asher, R. K., Benjamin, D. W., Bennett, L K., Raub, C. J. (1994). *ASM Handbook*, Vol. 5.
- [53] Kelly, J. J. and Yang, Y. C. (2001). Electrodeposition of Ni From a Sulfamate Electrolyte, *Sandia National Laboratories Report SAND2001-8609*, pp. 1-26.
- [54] Lowenheim, F. A., & Davis, J. (1974). Modern Electroplating. *Journal of The Electrochemical Society*. <https://doi.org/10.1149/1.2402361>
- [55] Tian, Q. H., & Guo, X. Y. (2010). Electroless copper plating on microcellular polyurethane foam. *Transactions of Nonferrous Metals Society of China (English Edition)*, 20(SUPPL.1), pp. 283–287. [https://doi.org/10.1016/S1003-6326\(10\)60057-X](https://doi.org/10.1016/S1003-6326(10)60057-X)
- [56] Singh, Y. (2013). Electrical Resistivity Measurements: A Review . *International Journal of Modern Physics*. Vol 22 pp. 745–756. <https://doi.org/10.1142/S2010194513010970>
- [57] Langford, J. I., & Wilson, A. J. C. (1977). Scherrer after Sixty Years: A Survey and Some New Results in the Determination of Crystallite Size. *Journal of Applied Crystallography*, Vol. 11. pp. 102–113.
- [58] Klug, H. P., & Alexander, L. E. (1974). Crystallite-Size Determination from Line Broadening. *X-Ray Diffraction Procedures: For Polycrystalline and Amorphous Materials*. 2nd Edition, Wiley .
- [59] Patterson, A. L. (1939). The scherrer formula for X-ray particle size determination. *Physical Review*, Vol. 56, pp. 978–982. <https://doi.org/10.1103/PhysRev.56.978>
- [60] Bragg, W. H., & Bragg, W. L. (1913). The Reflections of X-Rays by Crystals. *Proceedings of the Cambridge Philosophical Society*, Vol. 17 (1), pp. 428-438.
- [61] Schwartz, M. (2010). Deposition from Aqueous Solutions : An Overview. pp. 506-616.

- [62] Sapkal, S., Bhagwat, A., Bendrikar-Shinde, D., Vadhwania, Z., Gondil, R., Waikar, R., & Deshpande, M. (2015). Parametric Analysis of Electroless Nickel Plating- A Review. *National Conference on, Modeling, Optimization and Control*.
- [63] Conwell, E., & Weisskopf, V. F. (1950), Theory of impurity scattering in semiconductors, *Physical Review*, 77(3), pp. 388–390.
- [64] Rutherford, E. (2012). The scattering of α and β particles by matter and the structure of the atom. *Philosophical Magazine*, Vol. 92, pp. 379–398. <https://doi.org/10.1080/14786435.2011.617037>
- [65] Haitjema, H., Elich, J. J. (1991). Physical Properties of Pyrolytically Sprayed Tin-Doped Indium Oxide Coatings. *Thin Solid Films*, 205, pp. 93–100.
- [66] Chattopadhyay, D., & Queisser, H. J. (1981). Electron scattering by ionized impurities in semiconductors. *Reviews of Modern Physics*, 53(4), pp. 745–768. <https://doi.org/10.1103/RevModPhys.53.745>
- [67] Ioffe, L. B., & Wiegmann, P. B. (1990). Linear temperature dependence of resistivity as evidence of gauge interaction. *Physical Review Letters*, pp. 65(5), 653–656. <https://doi.org/10.1103/PhysRevLett.65.653>
- [68] Mössbauer, R. L. (1962). Recoilless nuclear resonance absorption of gamma radiation. *Science*. <https://doi.org/10.1126/science.137.3532.731>
- [69] Kip, A. F., & Kelley, J. B. (1970). Fundamentals of Electricity and Magnetism. *Physics Today*. <https://doi.org/10.1063/1.3022082>
- [70] Yamada, K., Shinozaki, B., Narikiyo, T., Takigawa, Y., Kuroda, N., Bando, T., & Nakamura, H. (2019). Temperature dependence of mobility of conducting polymer polyaniline with secondary dopant. *Synthetic Metals*. <https://doi.org/10.1016/j.synthmet.2018.11.019>
- [71] Kwoka, M., Ottaviano, L., Passacantando, M., Santucci, S., Czempik, G., & Szuber, J. (2005). XPS study of the surface chemistry of L-CVD SnO₂ thin films after oxidation. *Thin Solid Films*. <https://doi.org/10.1016/j.tsf.2005.04.014>
- [72] Malburg, M.C.; Cohen, D.K.; Lo, M. (2002). *ASME B46.1 2002 Surface Texture (Surface Roughness, Waviness, and Lay)*. New York.
- [73] Motta, M., Casselli, G. (2018). Eng Black Corintho 1100 St. *Duna Corradini Foams & Chemicals SPA*.
- [74] Singh, A. K. (2005). *Advanced X-Ray Techniques in Research and Industry*. IOS Press Publication.
- [75] Scardi, P.; Leoni, M.; Delhez, R. (2004). Line broadening analysis using integral breadth methods: a critical review. *Journal of Applied Crystallography*, 37, pp. 381–390. <https://doi.org/10.1107/S0021889804004583>

- [76] Scardi, P.; Leoni, M. (2001). Whole powder pattern modelling. *Acta Crystallographica Section A Foundations of Crystallography*, A58, pp. 190–200.

APPENDICES

A. List of Chemicals

- ✓ High density Polyurethane Foam: BLACK CORINTHO 1100, Duna Corradini, Italy
- ✓ Nickel Sulphamate ($\text{Ni}(\text{SO}_3\text{NH}_2)_2 \cdot 6\text{H}_2\text{O}$): 63035981 Umicore, Belgium
- ✓ Nickel Chloride (NiCl_2): 339350 Sigma Aldrich
- ✓ Boric Acid (H_3BO_3): 1001659012 Merck
- ✓ Palladium(II) Chloride, Reagentplus 99%, Aldrich
- ✓ Tin(II) Chloride, 99.99+%, Aldrich
- ✓ Sodium Hypophosphite Monohydrate, Aldrich
- ✓ Acetic Acid (Glacial) 100% , Ph Eur,Bp,Jp,Usp,E 260
- ✓ Potasyum Permanganat , Extra Pure, Tekkim
- ✓ Sodium Phosphate, 96%, Aldrich
- ✓ Sodium Carbonate, Anhydrous 99.5%, Ph Eur , Bp , Jp , Nf, Isolab
- ✓ Sodium Acetate Trihydrate 99.5%, Extra Pure, Ph.Eur, Bp,Jp,Usp,Fcc,E262, Sigma
- ✓ Tri-Sodium Citrate Dihydrate 99%, For Analysis Acs,Iso,Reag. Ph Eur, Isolab
- ✓ Na_2EDTA , Sigma
- ✓ Glycine 99.7% Gr For Analysis, Isolab
- ✓ $\text{C}_2\text{H}_5\text{OH}$, Sigma

B. MATLAB Code for PPMS Measurement

```
delta = 0.0005;
R = readtable('R and R.xlsx');
R_1 = R(:,1);
R_2 = R(:,2);
R_3 = R(:,1) + R(:,2);
z_0 = 2 * log(2) ./ (pi .* R_3);
y = zeros(length(z_0),1);
z = zeros(length(z_0),1);
z(:,1) = z_0;
R_S = zeros(length(z_0),1);
Grenze = 300000;
loopnumber = 0;
for i = 2:Grenze
    loopnumber = loopnumber + 1;
    y(:,i) = 1 ./ exp(pi .* z(:,i - 1) .* R_1) + 1 ./ exp(pi .* z(:,i - 1) .* R_2);
    z(:,i) = z(:,i - 1) - (1 - y(:,i)) ./ (pi .* (R_1 ./ exp(pi .* z(:,i - 1) .* R_1) + R_2 ./ exp(pi .* z(:,i - 1) .* R_2)));
    error = (z(:,i) - z(:,i - 1)) ./ z(:,i);
    R_S = 1 ./ z(:,i);
    if error < delta
        break
    end
end
end
```